PULSED LIGHT SINTERING OF NANOMATERIAL INTERCONNECTS EMBEDDED INSIDE MOLDED PDMS

By

MUKUND RAJEEV JOSHI

A thesis submitted to the

School of Graduate Studies

Rutgers, The State University of New Jersey

In partial fulfillment of the requirements

For the degree of

Master of Science

Graduate Program in Mechanical and Aerospace Engineering

Written under the direction of

Dr. Rajiv Malhotra

and approved by

_____

_____

_____

New Brunswick, New Jersey

May 2019

ABSTRACT OF THE THESIS

Pulsed Light Sintering of Nanomaterial Interconnects Embedded Inside Molded PDMS

By Mukund Joshi

Thesis Director:

Dr. Rajiv Malhotra

The need for flexible interconnects embedded inside elastomers is on the rise since the past few decades. This research explores how Intense Pulsed Light (IPL) sintering of interconnects consisting of Ag nanoflake-nanowire mixtures inside PDMS affects the electrical resistivity of the interconnect. Aerosol Jet Printing (AJP) was used to print the nanomaterial onto flexible PDMS substrates. The nanomaterial was encased by molding another layer of PDMS on top of it. IPL sintering was performed on the interconnect before and after molding the top PDMS layer, in two separate approaches. The IPL parameters and the nanoflake-nanowire ratio were varied to study their effect on sample quality. The fabricated samples were subjected to cyclic bending tests up to 1000 cycles. It is shown that there is an optimal fabrication route, with optimal IPL parameters and nanoflake-nanowire ratio that allows resistivity of around 9.75 - 11 μΩ-cm, with low hysteresis over 1000 cycles.

DEDICATION

This thesis is dedicated to my family, friends and faculty that were by my side throughout my Masters program.

First and foremost, I have to thank my parents for their love and support. My uncle, aunts and cousin deserve my whole-hearted thanks as well, for being there for me through thick and thin. You gave me the motivation to chase my dreams.

I would also like to thank my friend and roommate Anish for being by my side from the past three years. Also, my friend Sharva, who was always there for me whenever I needed him. The both of you have been my pillars of strength.

Lastly, I would like to thank my advisor Dr. Rajiv Malhotra for his unconditional support and guidance. This thesis would not be possible without the advice and expertise you shared with me over the course of this research. I offer my gratitude to all my colleagues from Dr. Malhotra's lab. Michael, Dr, Hwang, Harish, Naim and Jeremy, all of you have been big contributors to this research.

I thank all of you from the bottom of my heart for making this possible.

TABLE OF CONTENTS

LIST OF TABLES

LIST OF ILLUSTRATIONS

Chapter 1

Introduction

1.1 Applications of flexible interconnects

In recent years, flexible interconnects have found application in various products, creating a new domain of electronics called Stretchable Electronics. The most prominent of these include the manufacture of flexible displays for smartphones and TVs, organic transistors, organic light-emitting diodes [1], strain sensors having potential applications in sports performance analysis, medical rehabilitation and healthcare [2-6], wearable electronics [2, 7-11], in human-machine interfaces [12,13] as well as soft robotics [14-17].

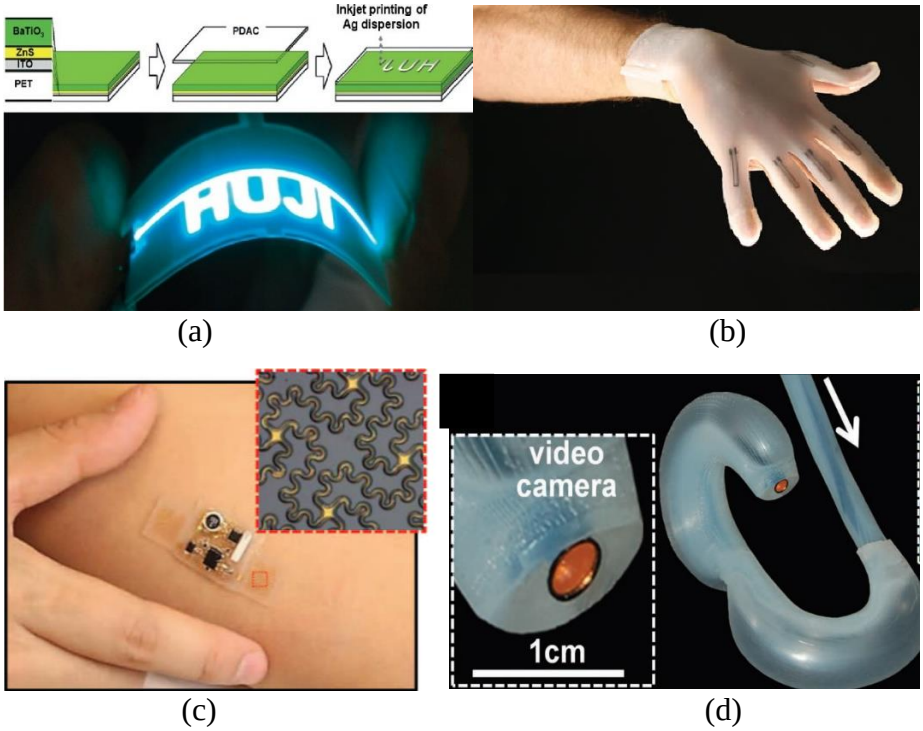

(a) (b)

(c) (d)

Fig 1. Applications of flexible interconnects in (a) Printed electronics such as flexible OLEDs [1], (b) Strain sensors for medical rehabilitation [6], (c) Wearable electronic sensors for measurement of Electrocardiograms (ECGs), Electroencephalograms (EEGs) and body temperature [11], and (d) Soft robotics for invasive surgeries [15]

1.2 Overview on the processes used to manufacture flexible interconnects

While flexible interconnects have a plethora of applications, their manufacturing poses a challenge. It is necessary to be able to mass-manufacture these interconnects in less time in order to make them inexpensive and cost effective. This can be done by the manufacturing techniques such as ink-jet printing or roll-to-roll processing. The choice of material for the conducting medium and elastic medium also determine the manufacturing feasibility of such flexible interconnects.

Metal nanoparticles or conductive graphene oxide are the preferred conductive media employed in making flexible interconnects owing to their superior electrical conductivity [18]. For the stretchable substrate, polymeric elastomers are preferred such as Eco-Flex or PDMS. Owing to their low elasticity modulus, these materials allow the easy deformation of the manufactured interconnects. A common method of manufacturing flexible interconnects is to deposit the nanomaterial on top of the elastomers or embed it inside them to form composite structures. The adhesion can between the layers can be enhanced by treating the elastomers with chemical processes [19] or by exposing them to oxygen plasma treatment [20], UV light irradiation [21] etc.

After this is done, certain methods and strategies are employed to enhance the conductivity and transparency of these flexible composites. Electrical conductivity in these composites is dictated by inherent conductivity of the nanomaterial as well as the degree of formation of a junction between adjacent (or overlapping) nanomaterial particles. Usually, junction resistance is higher in as-deposited state and can be reduced if the nanoparticles are welded or fused to each other. This is done using techniques such as high-force pressing [22],

annealing [23], laser sintering [24], IPL (Intense Pulsed Light) sintering or by soldering with other materials [25].

Common approaches to creating such flexible embedded interconnects are described below:

1. Vacuum filtration [26,27]**:** This involves the synthesis or deposition of a nanomaterial matrix (singular or hybrid) on a temporary substrate, which is applied onto the elastomer. Vacuum is used to transfer the matrix from the temporary substrate to the elastomer, where it gets adhered or embedded into the surface of the elastomer.

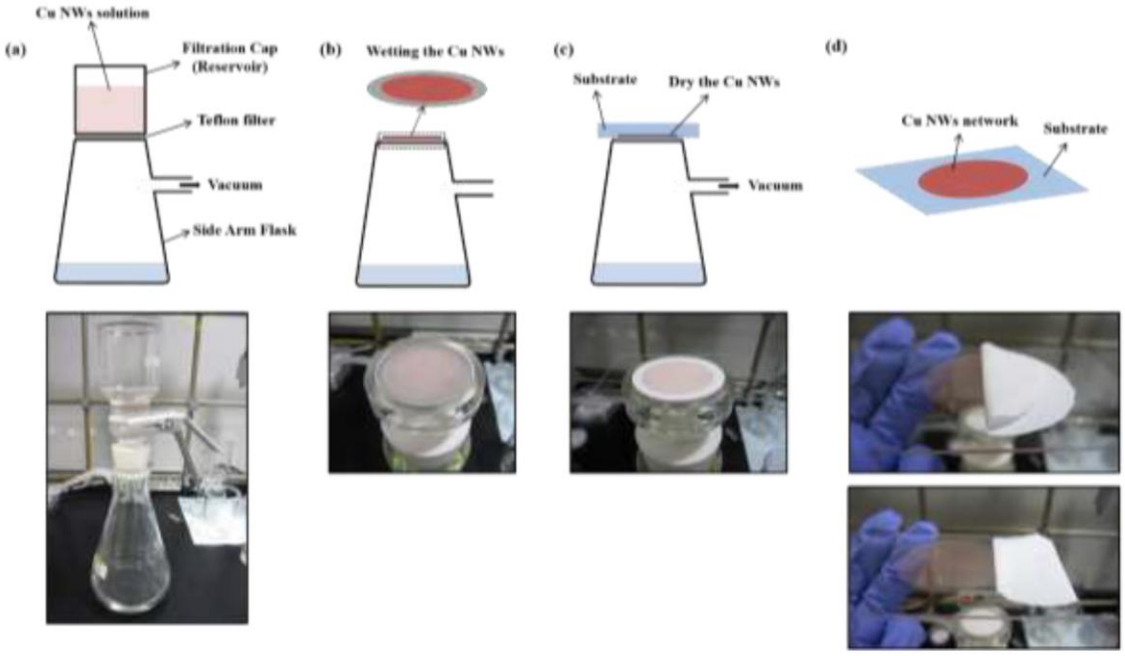

Fig 2. Schematic procedure of Vacuum filtration of Cu nanowires [26]

Han et.al. [26] use vacuum filtration as the transfer method to deposit Cu nanowires onto Ecoflex elastomer substrates. This paper describes the synthesis of a Cu nanowire percolation network, its transfer to flexible polyimide substrates and the use of laser

welding to reduce the oxidation of the Cu nanomaterial, and to reduce its resistance. The samples manufactured in this research had an initial sheet resistance of the order 10^3 to 10^9 Ω/sq. After sintering, the sheet resistance reduced to 20 Ω/sq. Cyclic folding and stretching tests were conducted to test the samples' performance during deformation. In cyclic bending, the samples were folded into an inverted V shape repeatedly. After 1500 folding cycles of this kind, the sheet resistance of these samples was around 50 Ω/sq. During cyclic stretching, the samples were subjected to repeated stretching from 0% strain to 250% strain, for 850 cycles. The samples, which were initially at a resistance of 300 Ω/sq before stretching, had a resistance of 360 Ω/sq after 800 cycles i.e. their resistance increases by around 20%.

2. Screen Printing [28, 29, 31]**:** In this method, nanomaterial inks (solutions of nanomaterial suspended in suitable solvents) are printed in patterns using a mask. This can be done by using a doctor blade or by an ink dispensing roller. Nanomaterial can be screen printed directly on elastomers, or on a temporary substrate. They are then transferred onto the elastomer by casting the liquid elastomer onto the pattern and allowing it to embed into the curing elastomer.

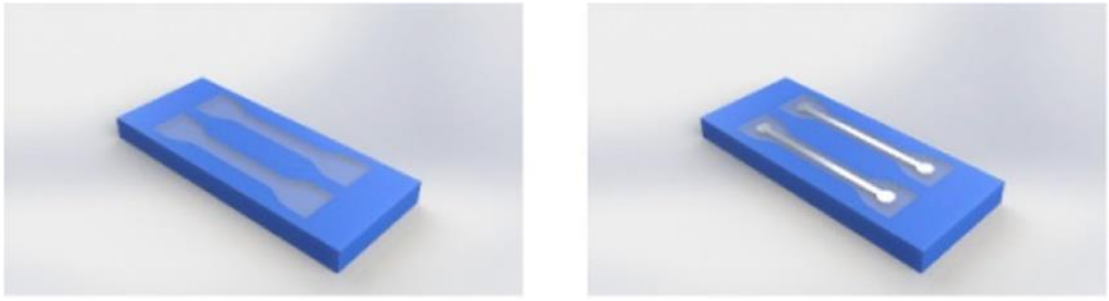

Fig 3. Schematic of screen printing of stretchable Ag nanoink on PDMS substrates [29]

Akash Shankar et.al. [29] used screen printing to deposit stretchable DuPont PE872 Ag nanoparticle ink on PDMS substrates. In this study, the authors described the effect of IPL sintering on the samples, to find out what IPL fluence (in J/cm^2) facilitates samples that can withstand maximum tensile strain without losing conductivity. The printed nanomaterial area in these samples was 2 mm x 30 mm in size.. The best samples in this study exhibited a resistance of 21 Ω before sintering, and 7.5 Ω when sintered at an IPL fluence of 20 J/cm^2.When subjected to tensile strain these samples failed at 27% strain during a single stretching cycle. The resistance at the time of failure was 67.5 Ω i.e. the samples had a $\Delta R/R_o$ value of 800% right before loss of conductivity.

3. Embedding nanomaterial inside liquid elastomer [30]**:** This process involves suspending nanomaterial (singular or hybrid) in liquid uncured elastomer to create a conductive paste. This paste can then be cast into interconnects using molds or can be applied between cured elastomer strips.

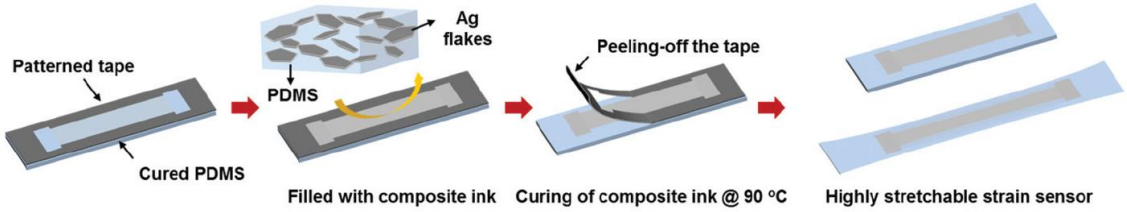

Fig 4. Deposition of nanomaterial embedded PDMS on pure PDMS substrate [30]

Inhyuk Kim et.al. [30] combined the use of such nanomaterial embedded elastomers with conventional screen printing, to deposit an Ag nanoflake-PDMS composite onto pure PDMS strips to obtain flexible interconnects. After depositing the conductive Ag-PDMS

paste on a pure PDMS strip using screen printing, the sample had to be thermally annealed at 90^{o}C for 2 hours. Following this, the samples were then sintered using IPL. When Ag flakes and nanocrystals (nanoparticles) were used in a 4:1 ratio, the samples had a conductivity of 2861 S/cm. These samples were stretched repeatedly upto 30% strain for 10000 bending cycles. The conductivity of the samples after bending dropped to approximately 2100 S/cm after stretching.

4. Embedded 3D Printing [32]**:** In this method, a nozzle extrudes a layer of nanomaterial ink inside a reservoir of uncured elastomer. The void created by the nozzle's motion is filled by liquid elastomer from the reservoir. Upon curing a composite with an embedded conductive element is obtained. After the elastomer is cured, it can be cut and extracted.

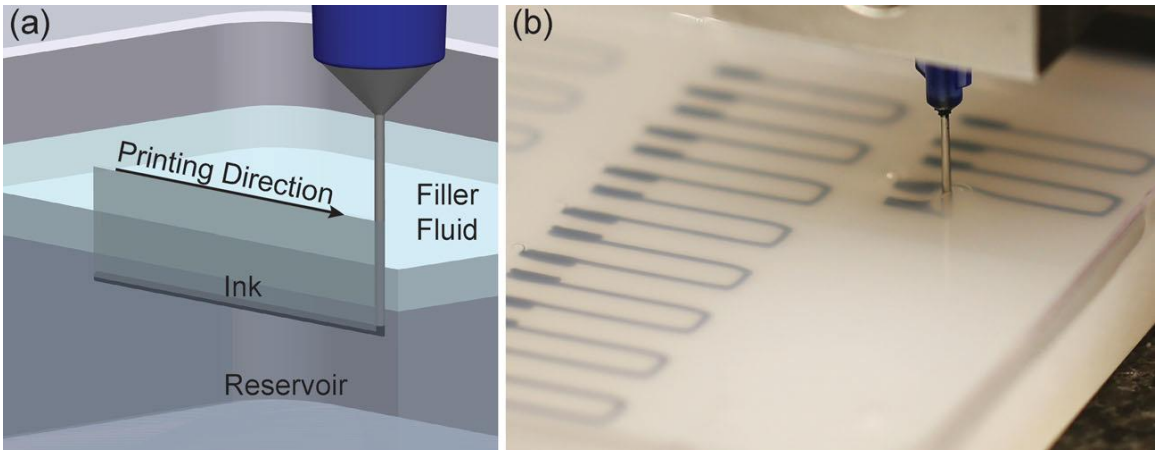

Fig 5. Embedded 3D printing of conductive Carbon ink in Ecoflex substrate [6]

Joseph Muth et. al. [6] used this technique to embed viscoelastic Carbon ink in Ecoflex elastomer substrates. The U-shaped printed patterns had a resistance of 11±2 kΩ in unstrained state. To test electrical performance as a function of cyclic straining, these samples were strained up to 100% strain over 5 stretching cycles. The resistance of these samples went up to 300 kΩ at 100% strain. Additionally, to test resistance at failure, the

samples were strained up to 450% strain. During a single stretching cycle, the samples showed a resistance of around 1.3 MΩ at 450% strain.

Evidently, the choice of material for the conductive element and elastomer, the transfer process and the techniques implemented to enhance conductivity of samples affect the static and dynamic resistivity.

1.3 Scope of this research

This research aims to examine how the nanomaterial composition of printed interconnects and a rapid Intense Pulsed Light (IPL) sintering approach to fuse the nanomaterials, affects the conductivity and cyclic bending behavior of interconnects embedded inside molded PDMS. Ag nanomaterial ink (consisting of a combination of Ag nanoflakes and Ag nanowires) is printed on molded PDMS substrates using a large-area Aerosol Jet Printer (AJP). Cu tape contacts are attached on these samples. The printed nanomaterial layer is then sandwiched by adding another layer of cured PDMS (i.e. Over-Molding). The conductive interconnect is then subjected IPL sintering before over-molding (Approach 1), and in a separate case after over-molding (Approach 2) as well, as shown below:

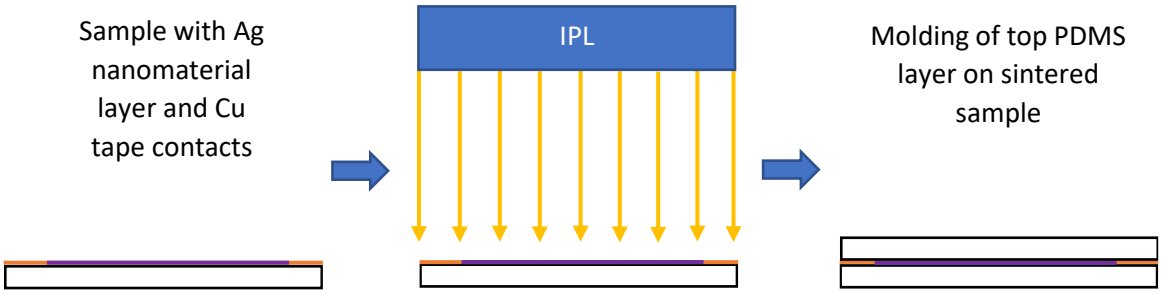

(a) Schematic of IPL sintering for Approach 1

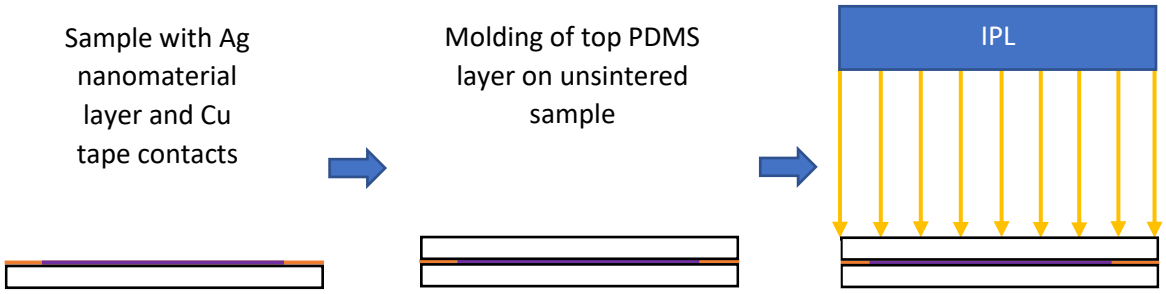

(b) Schematic of IPL sintering for Approach 2

Fig 6. Schematic showing the two approaches used to manufacture flexible interconnects

IPL has generated significant interest as a process that can be used for rapid and scalable sintering of nanomaterial [42]. IPL uses broad-spectrum, pulsed or continuous, light from a xenon lamp incident onto nanomaterial deposited on a substrate. The incident optical energy is converted into heat by the nanoparticles resulting in rapid densification of the nanoparticles. The key advantage of photonic sintering over conventional nanoparticle sintering processes is faster sintering of nanoparticle inks, about a few tens of seconds, over large area substrates (demonstrating an optical footprint of 0.75"x12" or greater) under ambient conditions [43]. It has been reported that IPL can minimize thermally induced damage to temperature sensitive substrates [44] and can increase adherence of the sintered nanoparticle film to the underlying substrate [40]. Due to the above qualities, IPL is amenable to integration with roll-to-roll and printing based techniques for high-speed and flexible manufacturing of the above devices.

The following effects of processing approach and nanomaterial composition on the as-fabricated resistivity and dynamic resistivity during 3 point bending around a 5 mm radius were documented in this project:

1. **Effect of Ag NF:NW ratio:** Different ratios of Ag NF:NW by weight were tested ranging from 80% Ag nanoflake - 20% Ag nanowire to 20% Ag nanoflake – 80% Ag nanowire.
2. **Effect of different molding approaches:** To examine the influence of molding, the samples were manufactured in two separate ways as shown in Figure 6.
3. **Effect of IPL parameters:** Typically, sintering nanomaterial via IPL shows a resistivity curve as shown in Figure 7. This curve has an optimum lowest resistance, after which the resistance of the nanomaterial increases. This is because using a higher fluence can damage the sample by causing the nanomaterial to blow off. To investigate this, the optimal pulse fluence sequence for samples of different NF:NW compositions was determined

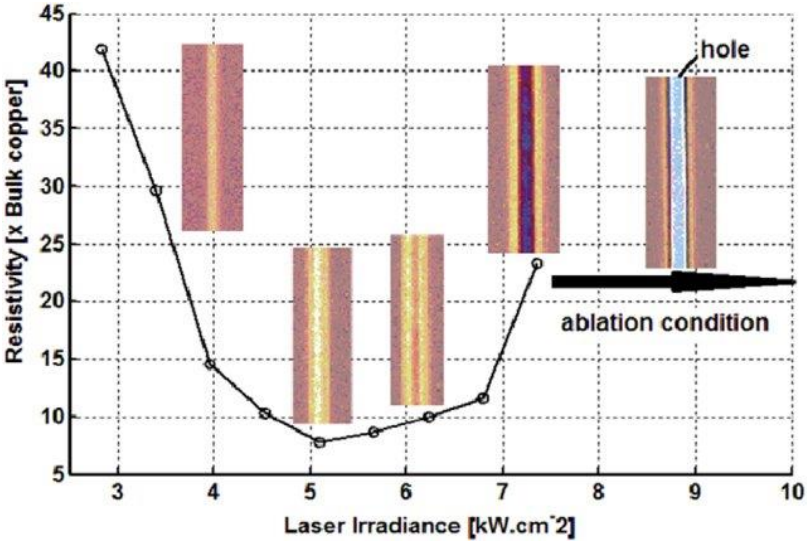

Fig 7. Typical resistance curve obtained during IPL sintering [47]

Further, these effects have been characterized in terms of their electrical resistance as follows:

1. Resistivity of the (processed) interconnect in static condition (R)

2. Change in resistivity of the interconnect during deformation (ΔR)

3. Electrical Hysteresis of the interconnect after 1000 bend cycles ($\Delta R'$)

Chapter 2

Experimental Procedure

2.1 Ink Preparation

Here, the term ‘ink’ refers to stable suspensions of silver (Ag) nanomaterial in ethanol. Silver was chosen as the choice of nanometal owing to high electrical conductivity, lesser corrosion than copper and easier dispersion than carbon-based nanomaterials. For choosing the solvent, the Ag nanomaterial was added to distilled deionized water, isopropanol (IPA), ethanol and tetradecane. It was observed that Ag nanomaterial suspended better in ethanol than the other solvents. Hence, ethanol was the choice of solvents for the inks in this research. Figure 8 shows the suspensions of Ag nanomaterial in these solvents.

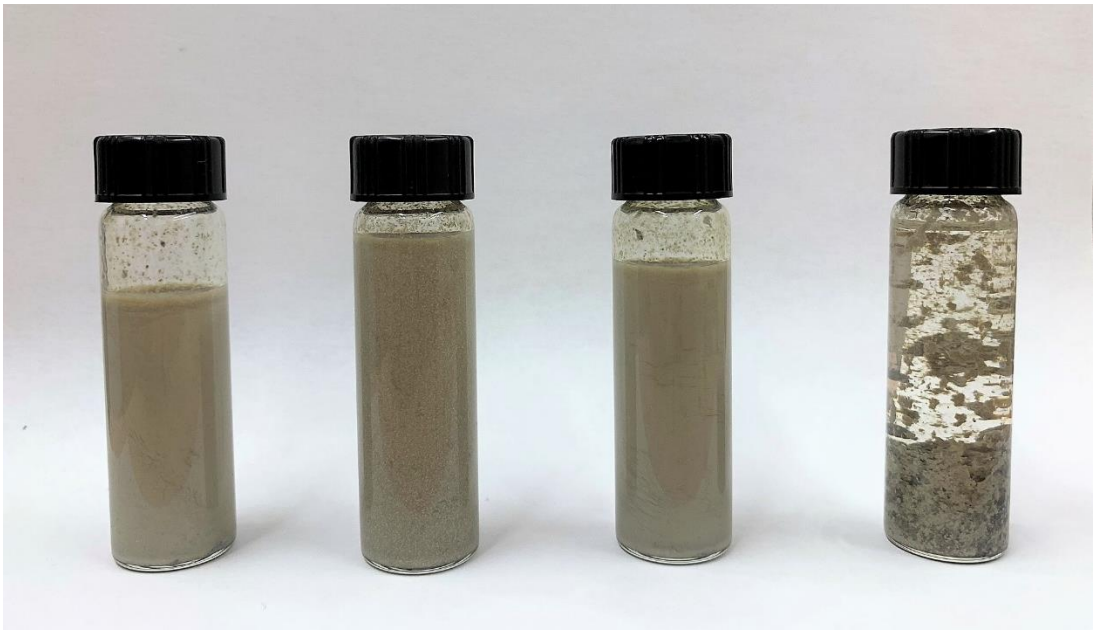

(a) (b) (c) (d)

Fig 8. Ag NF:NW inks in (a) DI water, (b) IPA, (c) Ethanol and (d) Tetradecane

Ag nanomaterial of 3 morphologies – Nanoparticles (spherical), Nanowires and Nanoflakes were considered for creating inks. Using these, there are 6 possible inks that can be made i.e. pure nanoparticle (NP) ink, pure nanowire (NW) ink, pure nanoflake (NF) ink, nanoparticle-nanoflake (NP:NF) ink, nanoparticle-nanowire (NP:NW) ink and nanoflake-nanowire (NF:NW) ink. To make a choice on the type of Ag nanomaterial, the possible implications of using these different morphologies were considered from the perspective of their interaction with each other in terms of bending.

Out of the three, nanoparticles are spherical and have the least surface area. A spherical Ag nanoparticle can only have point contact with an adjacent/overlaying nanoparticle. When the interconnect is bent, this point contact can be easily broken, leading to a break in the electrical circuit established by the Ag nanomaterial. Due to this, nanoparticles are a poor choice of nanomaterial.

Nanoflakes, on the other hand have a larger surface area due to larger in-plane dimension (the nanoflakes used had an in-plane dimension of 200-300 nm and a thickness of 20-30 nm). Due to this, overlapping nanoflakes will have area contact, and can slide against each other, maintaining electrical contact even when embedded conductor is deformed. Nanowires are long in length and can establish contact with multiple nanoflakes at the same time. When deformed, nanowires can still be in contact with them, thus ensuring stable electrical contact. Due to this, nanoflakes and nanowires were chosen as the nanomaterials investigated here.

The Ag inks were made by adding 2% by weight of nanomaterial to ethanol. Ratios of NF to NW were varied to create different inks. In the work, we use inks of NF:NW weight ratios 80:20, 60:40, 40:60 and 20:80 respectively.

In these ratios, the Ag nanomaterial stays relatively well suspended in ethanol, to form stable solutions. The nanomaterial stays suspended for around 4 -6 hours, without any need for intermittent ultrasonication or mixing. A larger amount of nanomaterial loading can be used by adding small portions (<10% by weight) of Polymer Dispersant/Surfactant. Using dispersant ensures that the higher nanomaterial concentration stays suspended. However, when this ink is sintered, the dispersant burns, staining and damaging the samples and subsequently affects its resistance [48]. Hence, dispersant was not added in the making of these inks.

2.2 Elastomer Strip Preparation

PDMS was chosen to be the choice of elastomer, due to its frequent use in flexible electronics [2, 9, 19, 30]. Dow Sylgard 184 PDMS comes in a two-part mixture, an elastomer liquid polymer and a curing agent. 10 parts of the liquid polymer and 1 part of the curing agent were mixed by weight. The mixture was then de-gassed in a vacuum chamber for 30 - 45 minutes to remove trapped air bubbles. After this, the mixture was poured into a mold made out of acrylic sheets and glass slides. This mold was coated with a layer of Mann Ease Release spray, which ensures that the PDMS does not stick to the mold after curing. The mixture poured into this mold was left to cure for 12 hours at room temperature (30ºC / 86º F). Then, the cured PDMS elastomer sheet was taken out of the mold. A thin layer of polycarbonate film was applied to one surface of the cured sheet, to prevent it from sticking to surfaces. After this, the PDMS sheet was cut into strips of 50 mm x 10 mm size. Each such strip was used to make one sample. This procedure is illustrated in Figure 9 below.

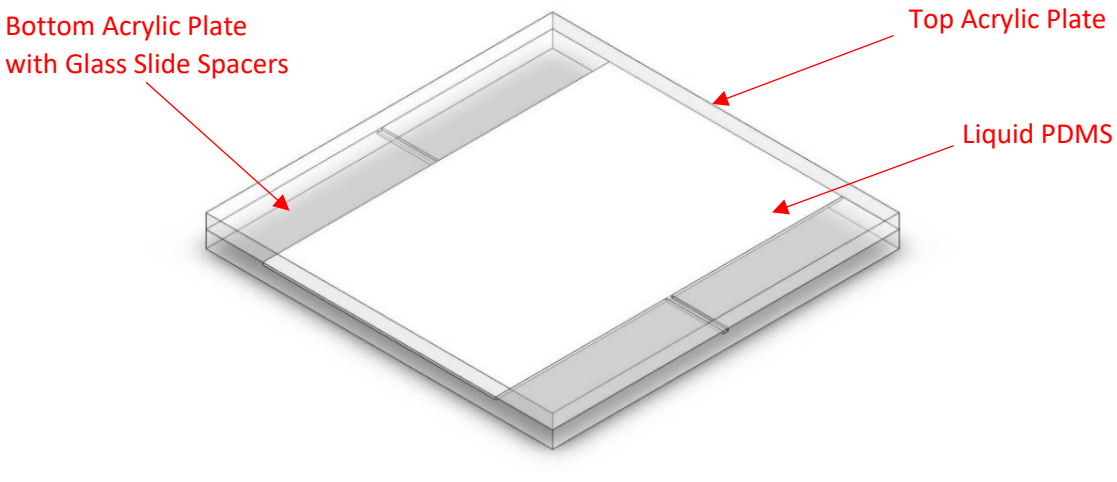

(a)

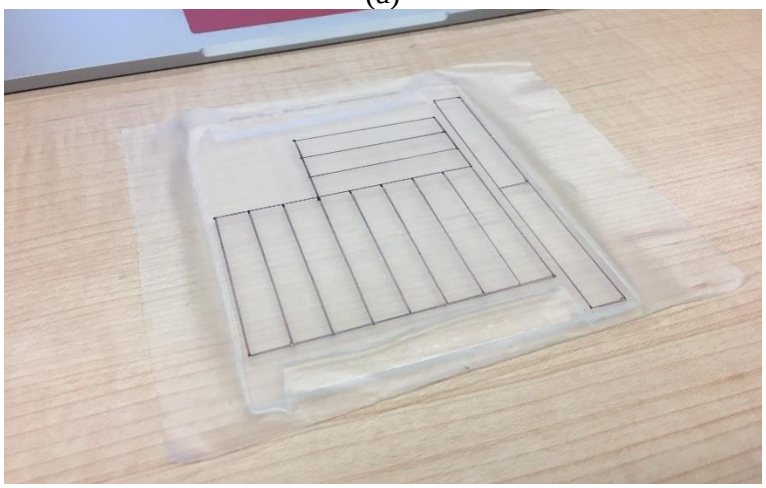

(b)

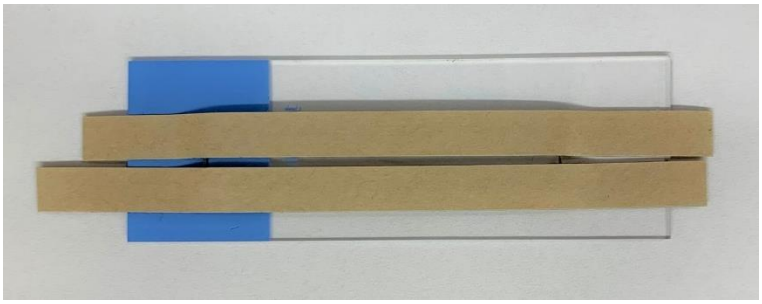

(c)

Fig 9. (a) Schematic of casting liquid PDMS into sheets, (b) Cured PDMS sheet with thin plastic film and markings, (c) PDMS strip with 1 mm wide tape-pattern

The strip was placed with the polycarbonate sheet facing down on a glass slide. On the top surface, a pattern was made using standard double-sided tape. The pattern was such that it leaves a 1 mm wide strip of PDMS exposed along its length. This 1 mm wide pattern would then be sprayed with nanomaterial under the Aerosol Jet Printer.

2.3 Aerosol Jet Printing

This step involved the deposition of Ag inks onto the patterned samples. The Aerosol Jet Printer (AJP) atomizes liquids to disperse them. This method is superior than screen printing because it allows the deposition of very fine layers of liquid [49,50]. Also, AJP has an advantage over vacuum filtration transfer techniques as it does not involve any transfer process.

As seen in Figure 10, the AJP consists of a movable X-Y stage. This stage is temperature controlled, in order to keep the samples at a fixed high temperature. A Z stage is mounted with the nozzle, and the nozzle has an ultrasonic atomizer which vibrates at a high frequency to atomize dispensed fluid. The nozzle is connected to a syringe pump that provides a regulated flow of ink to the nozzle.

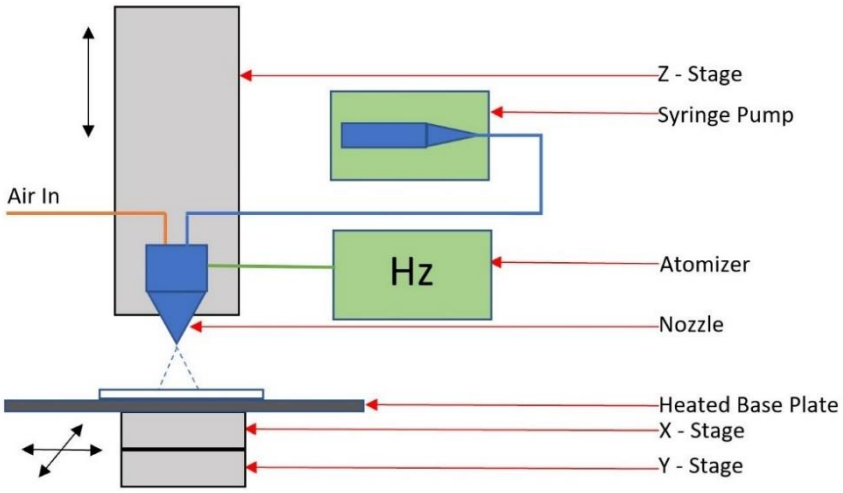

Fig 10. Schematic of Aerosol Jet Printing (AJP) setup

The X-Y stage was kept at a temperature of 85^{o}C (185^{0}F) in order to evaporate the ethanol from the ink almost instantly after it was deposited on the sample. The atomizer nozzle was kept at a height of 1 inch from the samples. The ink was loaded into the syringe and dispensed with a flow rate of 1.5 ml/min. The X-Y stage was moved in a linear motion at a speed of 50 mm/s to expose the sample to a series of 'passes' under the nozzle. This was done by using G-code to create a specific trajectory of travel for the printing plate. Each sample underwent 50 passes under the nozzle, which amounts to approximately 1.2 ml of ink deposition by volume. However, the AJP nozzle atomized the ink, making it spread out onto the printing plate. Thus, the actual quantity of Ag ink deposited onto the 1 mm wide strip was much lesser. The strip was placed with the polycarbonate sheet facing down on a glass slide. On the top surface, a pattern was made using standard double-sided tape. The pattern was such that it leaves a 1 mm wide strip of PDMS exposed along its length. Thus, a 1 mm strip in the middle of the PDMS samples was coated with a fine layer of Ag nanomaterial, as seen below in Figure 11.

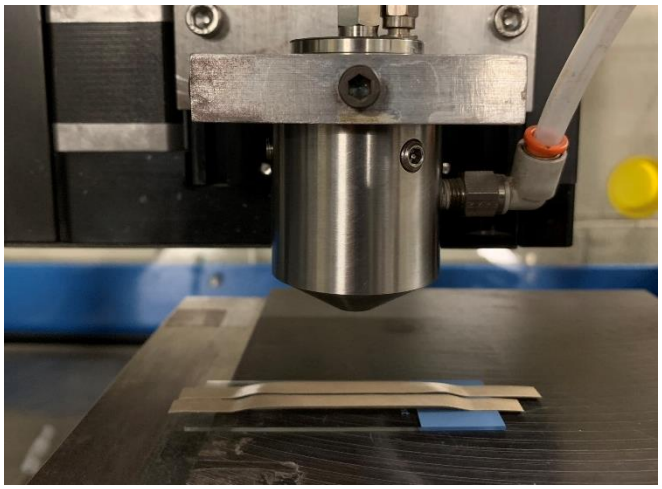

(a)

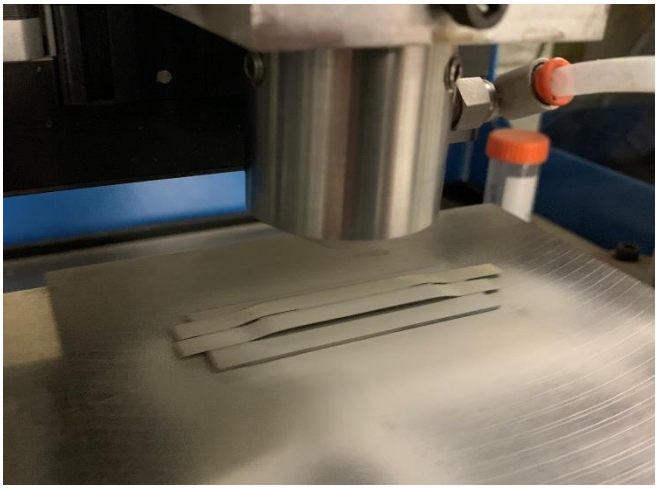

(b)

Fig 11. PDMS strip (a) before and (b) after AJP Printing

The two-wire method was used as the method of measuring resistance of the manufactured printed silver lines. To do so, adhesive Cu tape (of ¼" width) was attached to either ends of the Ag layer on the samples. The adhesive in this Cu tape was conductive. Approximately 20 cm of tape was used on either end of the samples. This added a resistance of around 367 mΩ to each sample, which was compensated for during resistance measurement. Samples in Approach 1 were sintered after this process. Then, the top PDMS layer was molded on these samples. On the other hand, the top PDMS layer was molded

onto samples in Approach 2 before IPL sintering. This procedure is illustrated in Figure12 below.

It is a common practice to use conductive pastes such as Ag amalgam while Cu tape is attached to various substrates. This is done in effort to minimize the contact resistance between the two surfaces. However, it was observed that Ag amalgam has very bad adherence to PDMS and the Cu tape contacts peeled of very easily when they were attached in this manner. Due to this, the Cu tape contacts were attached to the PDMS directly, without the use of Ag amalgam.

(a) (b)

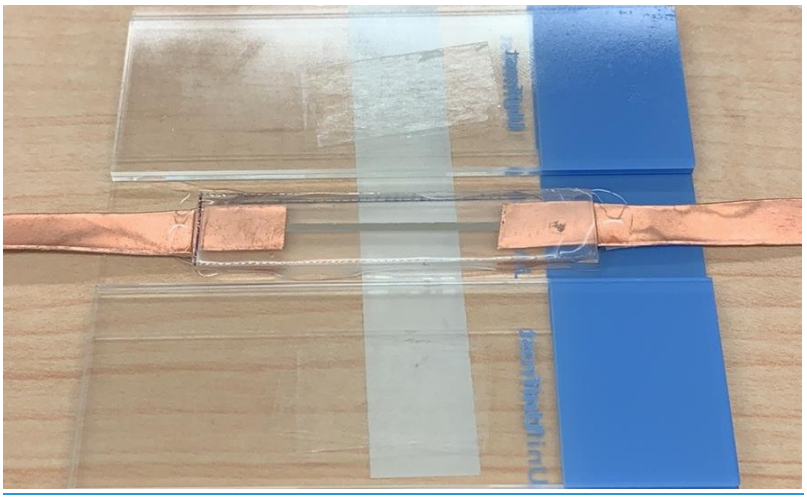

(c)

Fig 12. (a) PDMS strip with printed Ag nanomaterial, (b) Sample with Cu tape contacts, (c) Sample with top PDMS layer

2.4 Intense Pulsed Light (IPL) Sintering

IPL is suitable for most metals as the plasmon resonance of many metals is in the xenon lamp spectrum [33-37]. This form of sintering anneals (or welds) the nanomaterial almost instantly, requiring only milliseconds of light exposure. Also, IPL sintering involves only a few operational conditions such as irradiation time, pulse gap, pulse energy and pulse number to control the process. Due to these attributes, IPL sintering has been widely used in the field of solution based printed electronics for nanoparticle and nanowire sintering [38-41].

Here, IPL sintering was used to fuse the adjacent/overlapping nanoflakes and nanowires to each other. This was done to study the effect of IPL sintering on contact resistance and determine if IPL helps in improving electrical contact in static and dynamic conditions. After the samples were printed via the AJP technique and contacts were added, they were placed under the xenon lamp for IPL. Samples were not taken out of their molds during sintering. The lamp was at a fixed distance of 1 inch away from the interconnect samples. The samples were then exposed to a sequence of pulses of light of varying energy intensities (fluences). The lowest fluence used was 1 J/cm^2. Fluence was incremented in multiples of 1 J/cm^2. The resistance of the samples was obtained before sintering, and after each pulse light, to study the trend in change of resistance with increase in IPL fluence. The sequence of increasing fluences was terminated either if the sample lost conductivity during IPL sintering, or if the sample was at its lowest possible resistance at a certain fluence. Based on the optimal fluence sequence thus obtained, another sample was fabricated. These optimally sintered samples were taken out of their molds and used on the mechanical bending tester to test their electrical hysteresis during deformation.

For Approach 1 samples, the samples were directly sintered via IPL, with the Ag nanolayer facing the lamp. After sintering, another PDMS strip of same dimension was taken, and a thin film of liquid PDMS was poured on it. This strip was then placed on the printed sample, to 'sandwich' the Ag nanomaterial layer between both PDMS layers. The thin film of liquid PDMS serves as a 'glue' and allows the two PDMS strips to bond completely and fuse into a single casing for the Ag nanomaterial. These sandwiched samples were allowed to cure for 12 hours at room temperature (30^{o}C/86^{o}F), followed by IPL sintering. For Approach 2 samples, the same procedure was conducted to cover the samples with the second PDMS strip, but before IPL sintering.

2.5 Bending

The interconnects manufactured using above processes were subjected to 3-Point bending around a 10 mm diameter, on a tester to analyze their electrical hysteresis when subjected to multiple bending cycles.

A schematic of how the bending was conducted can be seen in Figure 13 :

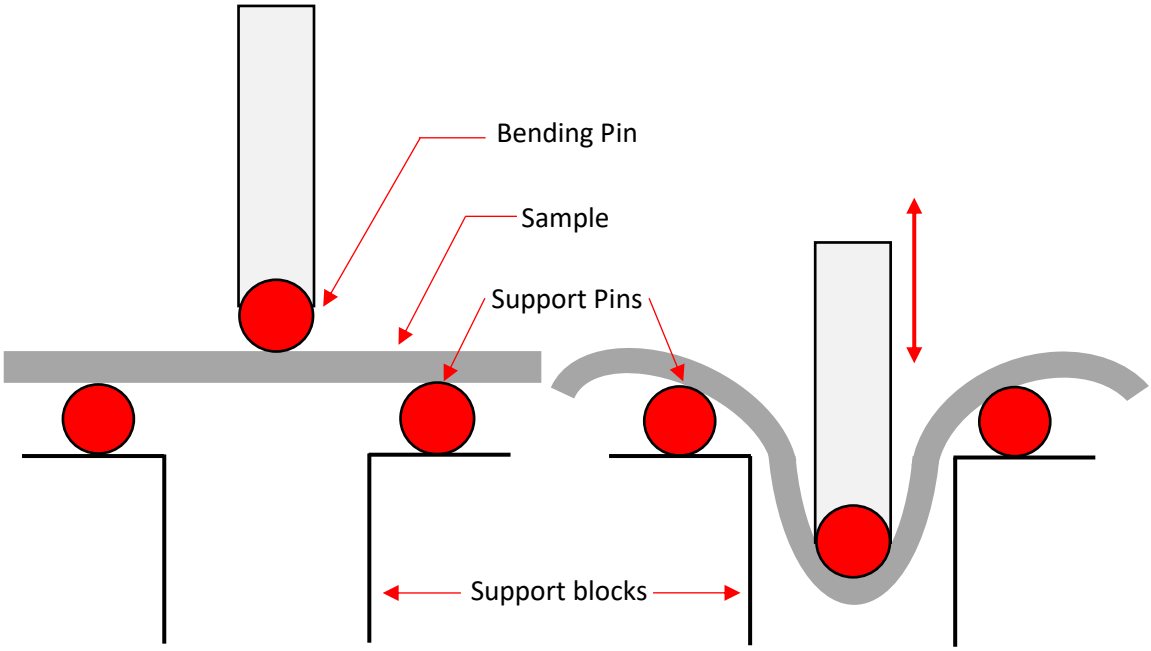

Fig 13. Schematic of 3-Point Bending of flexible interconnects (The 3 cylindrical pins used to support and bend the sample are shown in red)

A mechanical tester (shown in Figure 14) consisting of a vertically mounted linear translation stage, and attachments to hold the interconnect was built to conduct bending tests. This mechanical tester consisted of two support blocks that could slide on the base plate, to adjust the gauge length for bending. Cylindrical pins were mounted on these blocks, to act as supports for the interconnect sample. A transparent acrylic plate on the front and an aluminum back plate ensured that there was no lateral shifting of the sample during bending. A cylindrical pin mounted on an aluminum rod was attached onto moving platform of the linear translation stage. This pin had a 10 mm diameter, which was used to push into the interconnect to bend it. The interconnect sample was then connected to a Keithley 2400-C source meter to measure resistance. The tester and the source meter were

controlled by a laptop to perform 1000 bend cycles and detect changes in resistance during the process.

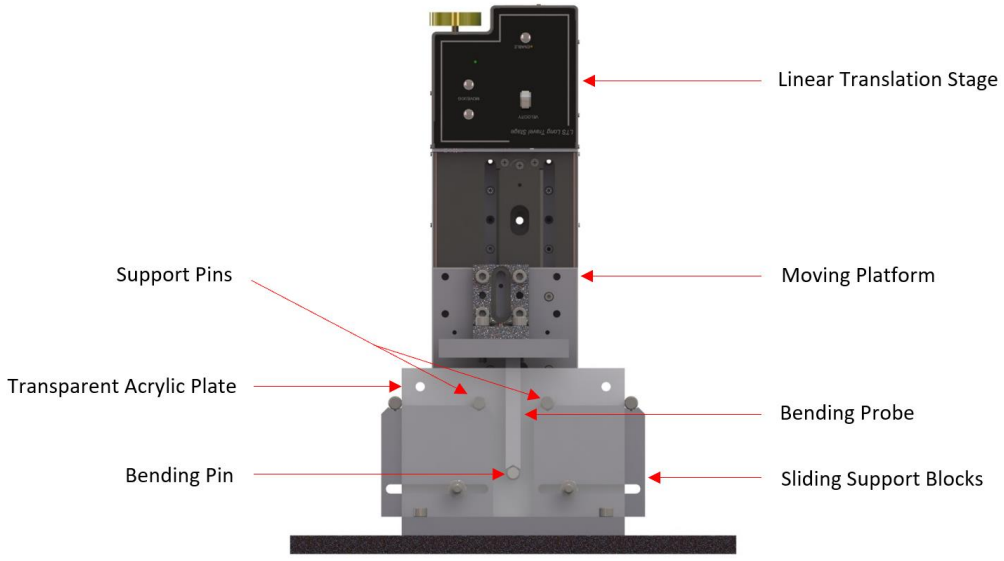

(a)

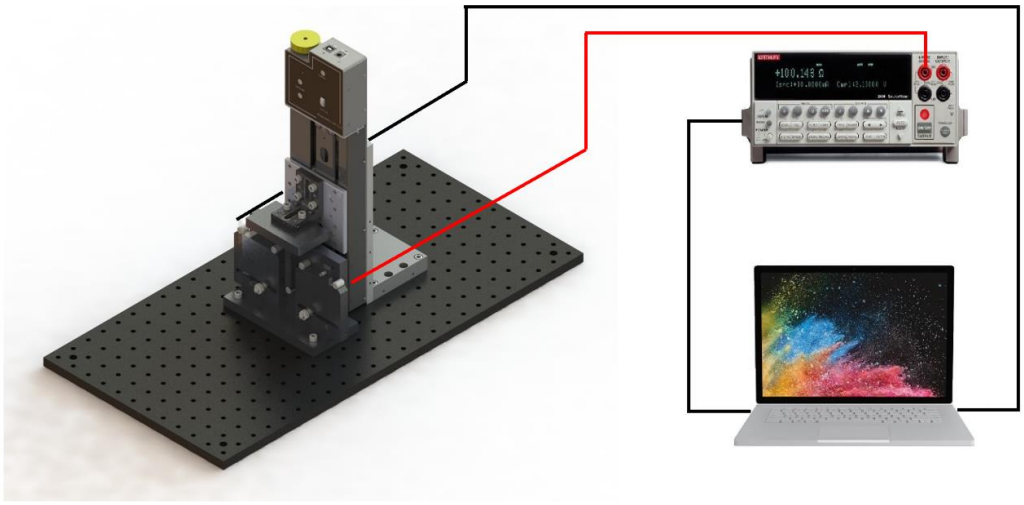

(b)

Fig 14. Schematic of Mechanical Bending Tester Setup showing (a) The parts in the bending tester and (b) Its assembly with the source meter

The samples were placed on the attachment such that they were supported by two dowel pins 1 inch apart. The samples have a thickness of 2 mm. The samples were bent until they formed a U-shape which involved deflecting the samples by a distance of 21 mm from the resting position.

The probe takes approximately 2 seconds to bend the interconnect, and 2 seconds to retract, thereby performing 1000 bends at a frequency of 0.25 Hz. Over the course of these 4 seconds, the source meter makes resistance measurements. The source meter was programmed to do a linear voltage sweep, with a voltage ranging from 0 V to 5 V and a current of 0.01 A. At these settings, 4000 measurements were conducted over the 1000 bends, at a time step of 1 second between successive readings.

Chapter 3

Results and Discussions

3.1 Bending of unsintered interconnects

As described in the Experimental Procedure (Chapter 2), IPL sintering was done on the samples before bending them. IPL sintering enhances the properties of the interconnects, by reducing the resistance of the Ag nanomaterial in the samples, while enhancing its ability to endure damage during mechanical deformation. However, it was necessary to confirm that IPL does induce these positive changes in the samples. To do so, samples that were not sintered via IPL were mounted on the bending tester, and their dynamic hysteresis was measured and analyzed. This test was conducted only on the Approach 2 – NF:NW 60:40 and 40:60 samples, as these were the best performing samples (described in Sections 3.3-3.6).

3.1.1 Bending of unsintered Approach 2 – 60:40 ratio sample

The Approach 2 – 60:40 sample chosen for unsintered bending had a resistance of 2.36 Ω/cm before addition of the top PDMS layer. Upon adding the top PDMS layer, its resistance increased to 2.64 Ω/cm. This sample had a resistance of 3.8 Ω/cm when it was mounted on the bending setup, right before the bending began.

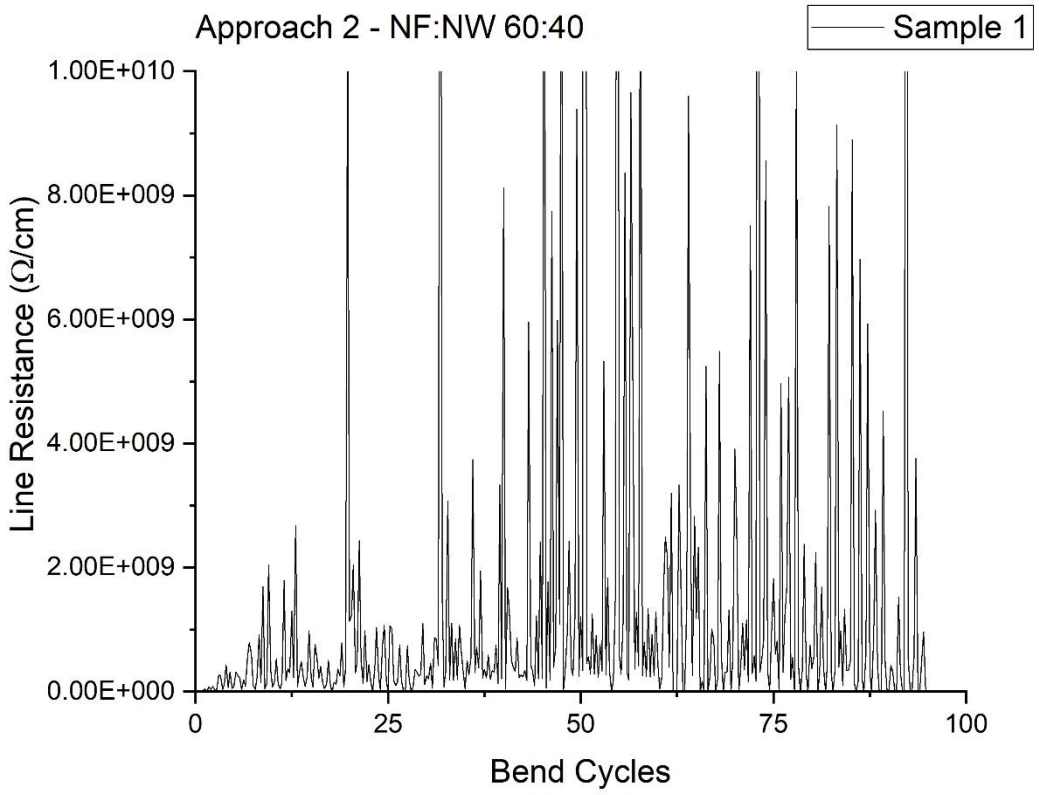

Fig 15. Dynamic hysteresis during bending for unsintered Approach 2 – NF:NW 60:40 sample

Figure 15 shows the performance of unsintered Approach 2 – NF:NW 60:40 sample during bending. It can be observed that the change in resistance during the bend-release cycles was very erratic and did not follow a specific trend. The readings in bent state show values in the order of 108 – 1010 Ω/cm. The sample lost conductivity after 92 bend cycles. Also, the sample showed no conductivity as soon as it was taken off the bending setup. This goes on to show that the samples did not show good results when subjected to bending right after manufacturing.

3.1.2 Bending of unsintered Approach 2 – 40:60 weight ratio sample

The Approach 2 – 40:60 sample chosen for unsintered bending had a resistance of 1.96 Ω/cm before addition of the top PDMS layer. Upon adding the top PDMS layer, its resistance increased to 3.06 Ω/cm. This sample had a resistance of 3.12 Ω/cm when it was mounted on the bending setup, right before the bending began. This sample lost conductivity as soon as the bending began, owing to high mechanical damage to the Ag nanomaterial layer. No readings could be recorded during bending. To confirm that this phenomenon was not a one-time error, another sample of the same configuration was manufactured and tested. The second sample showed the same behavior. This confirmed that the unsintered Approach 2 – NF:NW 40:60 sample does not survive bending.

3.2 Dynamic Resistance for Processing Approach 1

3.2.1 NF:NW 80:20 ratio

Two samples of NF:NW 80:20 weight ratio were documented. It was observed that the two samples were not similar in terms of resistance (as seen in Table 1 and Figure 16). They also reacted differently to IPL sintering. Sample 1 had a resistance of 30 Ω/cm before IPL sintering. Its resistance decreased to 25.2 Ω/cm when flashed with 1 pulse of fluence 1 J/cm^2 and further decreased to 23.6 Ω/cm after being pulsed with 1 pulse of fluence 2 J/cm^2. After this, the top PDMS layer was added to this sample. Upon curing, it was observed that the resistance increased to 19 MΩ. Sample 1 also lost conductivity when it was demolded and placed onto the bending tester. Sample 2 had an unsintered resistance of 45 Ω/cm. Contrary to the trend observed in Sample 1, the resistance of Sample 2 increased to 58 Ω/cm and then to 62 Ω/cm when subjected to a pulse sequence of fluences 1 J/cm^2 and 2 J/cm^2 respectively. This sample also lost conductivity after adding the top PDMS layer. This was because the Ag nanomaterial layer on the PDMS strip was partially blown off during IPL sintering.

Table 1. IPL Fluence Sequence and Resistances for Approach 1 – NF:NW 80:20 samples

	SAMPLE 1	SAMPLE 2
IPL Fluence (J/cm^2)	Line Resistance (Ω/cm)	Line Resistance (Ω/cm)
0	30	45
1	25.2	58
2	23.6	62
After Top Layer	19 x 10^6	∞

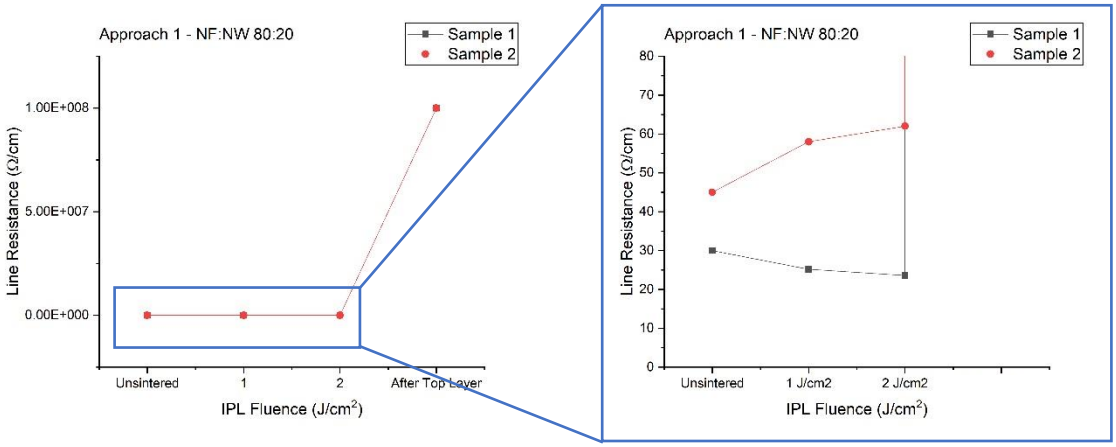

Fig 16. IPL – Resistance trends for Approach 1 – NF:NW 80:20 samples

Figure 16 shows the non-uniformity in the samples of the NF:NW 80:20 weight ratio. This was attributed to two possible reasons: (a) Inks with high concentrations of Ag nanoflake create a difficulty in deposition via AJP. It was observed that Ag nanoflakes tend to clog up the nozzle during deposition, leading to an uneven spray. This leads to deposition of Ag nanomaterial layers of unequal thicknesses in different samples. (b) Inks with higher Ag nanoflake concentrations show poor adherence to PDMS. Due to this, there is a high tendency of the Ag layer to be blown away during IPL sintering, as seen in Figure 17 below.

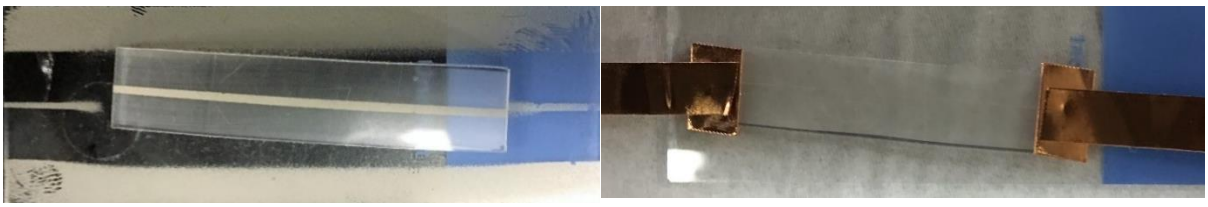

(a) (b)

Fig 17. (a) Distinct Ag nanomaterial layer seen on sample, (b) Ag nanomaterial layer blown off the PDMS strip during IPL sintering

3.2.2 NF:NW 60:40 ratio

Two samples of NF:NW 60:40 weight ratio have been documented for Approach 1. Upon IPL sintering it was observed that the lowest resistance were obtained after the samples were subjected to a pulse sequence of fluences 1,2 and 3 J/cm^2 respectively. Sample 1 had a low unsintered resistance of 2.8 Ω/cm. After the IPL pulse sequence, its resistance dropped to 2 Ω/cm. Upon adding the top PDMS layer, the resistance of Sample 1 increased to 8.2 Ω/cm. Sample 2 had an unsintered resistance of 4.2 Ω/cm. After the IPL pulse sequence, its resistance dropped to 2.78 Ω/cm.

Table 2. IPL Fluence Sequence and Resistances for Approach 1 – NF:NW 60:40 samples

	SAMPLE 1	SAMPLE 2
IPL Fluence (J/cm^2)	Line Resistance (Ω/cm)	Line Resistance (Ω/cm)
0	2.8	4.2
1	2.52	3.72
2	2.06	2.96
3	2	2.78
After Top Layer	8.2	7.6

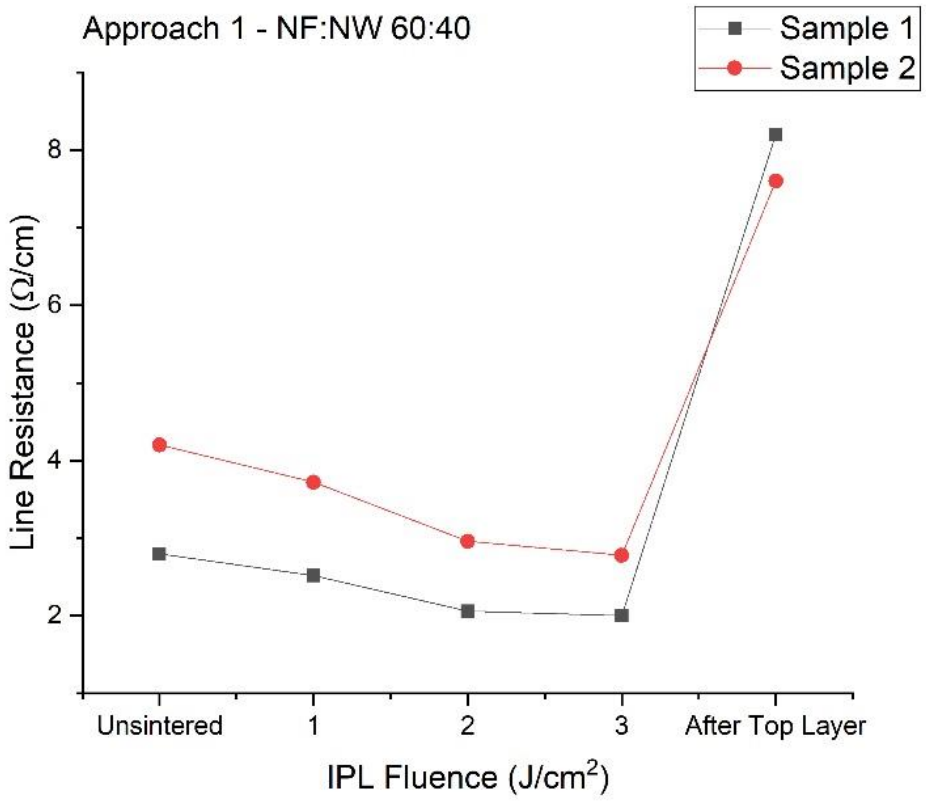

Fig 18. IPL – Resistance trends for Approach 1 – NF:NW 60:40 samples

From Figure 18, it can be seen that both the samples show very similar trends of resistance change during IPL, and also after addition of the top PDMS layer. It can also be noted that the NF:NW 60:40 samples have very low resistance even before IPL sintering. The increase in resistance after adding the top PDMS layer is also minimal.

Figure 19 shows the performance of Sample 1 during bending. The resistance of the sample fluctuated around 39 Ω/cm. The trend line of change in resistance during bending is fairly linear and horizontal. The sample was stable up to 58 bend cycles, after which the resistance fluctuated inconsistently. After this, the sample lost conductivity. Figure 20 shows the performance of Sample 2 during bending. The resistance fluctuated around 41

Ω/cm, and the trend line was fairly linear in this case too. However, unlike Sample 1, the increase in resistance when the sample was in bent condition was not similar over multiple bends. Also, the resistance of the sample in unbent condition was also not similar, implying that Sample 2 was not as stable as Sample 1. Sample 2 lost conductivity after 69 bend cycles.

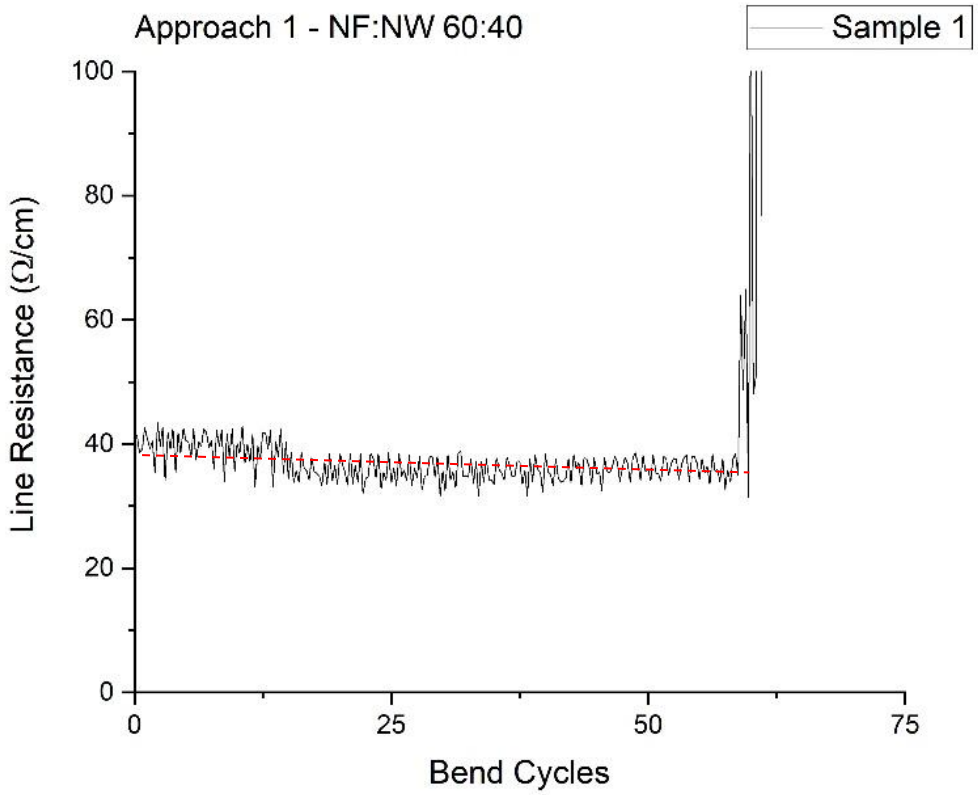

Fig 19. Dynamic hysteresis during bending for Approach 1 – NF:NW 60:40 Sample 1

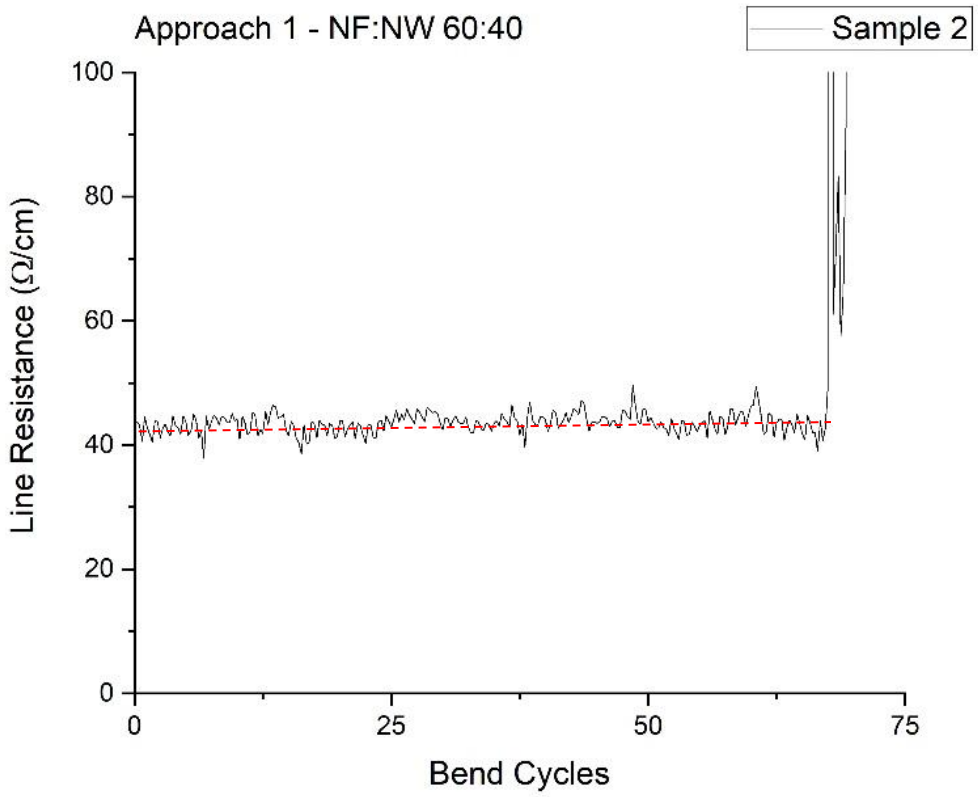

Figure 20. Dynamic hysteresis during bending for Approach 1 – NF:NW 60:40 Sample 2

These observations demonstrate that the NF:NW 60:40 weight ratio is more preferable than NF:NW 80:20, as it yields drastically lower resistance, and better performance in bending. However, the bending is not very consistent. Also, both the samples do not survive beyond 100 bends.

3.2.3 NF:NW 40:60 ratio

Two samples of NF:NW 40:60 weight ratio have been documented for Approach 1. Upon IPL sintering it was observed that the resistance of samples increased drastically when subject to a pulse sequence of fluences beyond 3 J/cm^2. Thus, the IPL pulse sequence was terminated after one pulse each of fluence 1 J/cm^2 and 2 J/cm^2. Sample 1 had a low

unsintered resistance of 3.86 Ω/cm. Upon IPL sintering, its resistance increased to 4.56 Ω/cm when exposed to 1 pulse of fluence 1 J/cm^2. Next, its resistance decreased to 4.36 Ω/cm after exposure to 1 pulse of fluence 2 J/cm^2. When the top PDMS layer was applied to Sample 1, its resistance drastically increased to 1.6 MΩ/cm. Showing a similar trend, Sample 2 had a resistance of 3.28 Ω/cm before IPL sintering. Its resistance increased initially to 3.62 Ω/cm and then decreased to 3.54 Ω/cm when sintered with IPL fluences 1 J/cm^2 and 2 J/cm^2 respectively. After adding the top PDMS layer, its resistance increased to 2.8 MΩ/cm.

Table 3. IPL Fluence Sequence and Resistances for Approach 1 – NF:NW 40:60 samples

IPL Fluence (J/cm^2)	SAMPLE 1 Line Resistance (Ω/cm)	SAMPLE 2 Line Resistance (Ω/cm)
0	3.86	3.28
1	4.58	3.62
2	4.36	3.54
After Top Layer	1.6 x 10^6	2.8 x 10^6

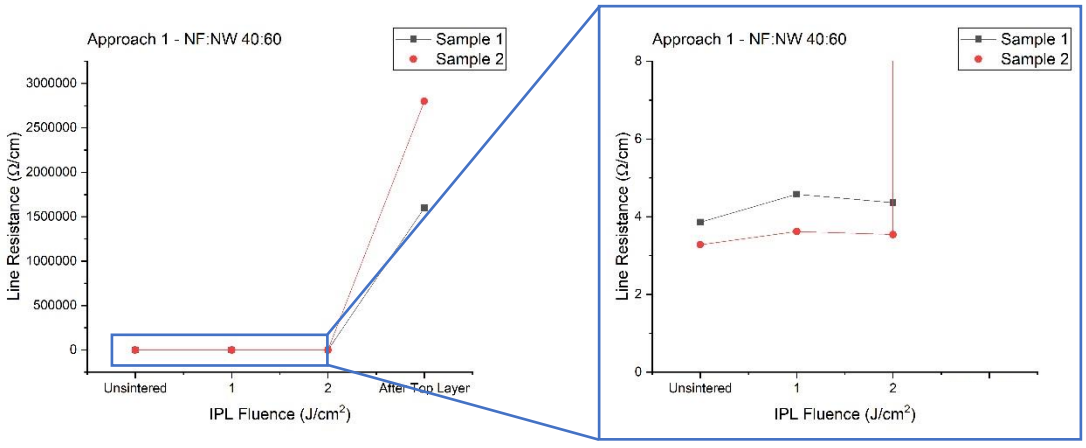

Fig 21. IPL – Resistance trends for Approach 1 – NF:NW 40:60 samples

Figure 21 shows the fairly similar similar behavior of both samples. The resistances of the NF:NW 40:60 samples can be compared to those of the NF:NW 60:40 samples, which are quite low. However, upon adding the top layer of PDMS, the resistance shoots up to very high numbers, rendering the NF:NW 40:60 samples bad candidates for flexible interconnects. As expected, removing the samples from their molds after IPL sintering and placing them into the bending set-up damages the samples. Due to this the samples lose conductivity completely before bending.

3.2.4 NF:NW 20:80 ratio

Two samples of NF:NW 20:80 weight ratio have been documented for Approach 1. Upon IPL sintering it was observed that the Ag nanomaterial layer was completely blown off the PDMS substrate when subject to a pulse sequence of fluences beyond 3 J/cm^2. Thus, the IPL pulse sequence was terminated after one pulse each of fluence 1 J/cm^2 and 2 J/cm^2. IPL sintering had a negative impact on these samples. Sample 1 had a resistance of 6.2 Ω/cm before IPL sintering. Its resistance increased to 8 Ω/cm after being put through an IPL pulse sequence of fluences 1 J/cm^2 and 2 J/cm^2 respectively. Adding the top PDMS layer increased the resistance to 4.4 MΩ/cm. Similarly, Sample 2 had a low unsintered resistance of 5.2 Ω/cm. After the pulse sequence, its resistance rose to 6.6 Ω/cm. Adding the top PDMS layer increased its resistance to 12.2 M Ω/cm. Figure 22 shows the fairly similar but poor trends of change in resistance in both NF:NW 20:80 ratio samples. IPL sintering increases the resistance of both samples. When taken out of their molds and placed onto the tester, the samples undergo damage and are unfit for dynamic resistance measurement during bending.

Table 4. IPL Fluence Sequence and Resistances for Approach 1 – NF:NW 20:80 samples

IPL Fluence (J/cm^2)	SAMPLE 1 Line Resistance (Ω/cm)	SAMPLE 2 Line Resistance (Ω/cm)
0	6.2	5.2
1	7.2	6.2
2	8	6.6
After Top Layer	4.4×10^6	12.2×10^6

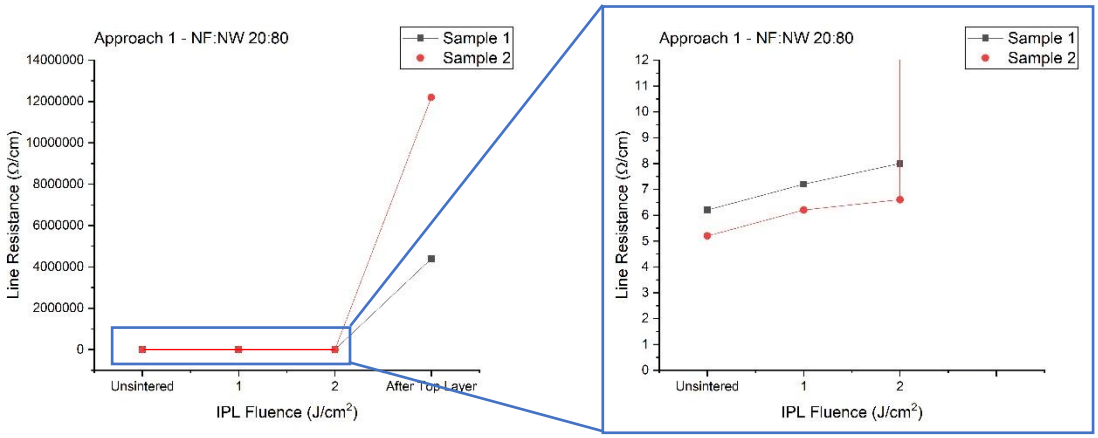

Fig 22. IPL – Resistance trends for Approach 1 – NF:NW 20:80 samples

3.3 Summary of Approach 1

Approach 1 involved IPL sintering of samples before addition of the top PDMS layer. After studying the performance of flexible interconnects manufactured by this approach, sample quality can be judged based on 4 criteria. Shades of grey have been used to describe the quality of the Ag nanomaterial ratios in these criteria, as seen in Table 5 below. White regions indicate good results, grey indicates average results and dark grey indicates poor results.

Table 5: Variation in sample quality for Approach 1 samples

	NF:NW			
	80:20	**60:40**	**40:60**	**20:80**
Resistance before IPL				
Resistance after IPL				
Resistance after adding top PDMS layer				
Low resistance during bending				

	Good		Fair		Bad

1. Resistance of samples before IPL sintering: Samples having higher concentrations of Ag nanoflakes have higher resistance, as compared to samples with moderate NF:NW weight ratios. This is because inks with high nanoflake content pose a difficulty during deposition. Inks with a high Ag nanoflake content have low viscosity. Ag nanoflakes are heavier than nanowires as they are larger in size. Thus, inks with high nanoflake content

do not suspend very well. Also, nanoflakes tend to clog the AJP nozzle creating problems during deposition. On the other hand, samples with high Ag nanowire content are highly conductive, and show low resistances before IPL. Samples with moderate NF:NW ratios have low resistances as well.

2. Resistance of samples after IPL sintering: It was observed that samples of NF:NW 60:40 weight ratio reacted favorably to IPL sintering. The resistance of NF:NW 60:40 samples decreases with increase in IPL fluence. Samples with NF:NW 80:20 weight ratio were very inconsistent in how they reacted to IPL sintering, showing different trends of change in resistance in both samples. This is because the deposition of nanoflakes causes clogging in the AJP nozzle leading to non-uniform deposition. Also, the Ag nanomaterial was blown off due to IPL sintering. Samples with NF:NW 40:60 weight ratio show an almost neutral response to IPL sintering. The resistance of these samples after sintering is almost the same as their resistance before sintering, indicating that IPL has little effect on them. This can be explained by the phenomenon discussed by Hwang et. al. in their paper, which states that an increase in Ag NW content in an ensemble inherently reduces the optical absorption efficiency of the nanomaterial [53]. Samples with NF:NW 20:80 react poorly to IPL sintering, as their resistance increases with increase in IPL fluence. Ag nanowire is more delicate as compared to Ag nanoflake. This is why samples with higher Ag nanowire content get damaged, showing high resistance after IPL. It is possible that there was some damage to the Ag nanowires in the NF:NW 40:60 case as well, due to which IPL sintering did not cause a significant reduction in resistance.

3. Resistance of samples after adding top PDMS layer: The addition of the top PDMS layer affects all samples, leading to an increase in resistance. This is because PDMS shrinks

during curing and while it does so, it exerts stress on the Ag nanomaterial ensemble by going into the inter-nanomaterial pores. This leads to an increase in resistance. Samples with inconsistently deposited nanomaterial are affected by this to a greater extent. Owing to this phenomenon, the resistance of samples with NF:NW 80:20 and 20:80 weight ratios goes into the MΩ range after adding the top PDMS layer . The NF:NW 40:60 samples also show a high resistance after the top layer was added, confirming that IPL sintering had damaged the Ag layer upto a certain extent, making it more fragile. The NF:NW 60:40 samples showed the smallest increase in resistance when the top layer was added, indicating that they were the best samples.

4. Low resistance during bending: It is necessary for the samples to have low resistance during bending, to be good candidates for use as flexible interconnects. An ideal flexible interconnect would show an almost horizontal trend when its resistance was plotted against repeated cyclic deformation, indicating that the resistance does not increase during deformation. The NF:NW 60:40 samples showed similar behavior, with a near horizontal trend line of resistance vs. bend cycles. However, the samples endured less than 70 bends.

3.4 Dynamic resistance for Processing Approach 2

3.4.1 NF:NW 80:20 ratio

Two samples of NF:NW 80:20 weight ratio have been documented for Approach 2. Upon IPL sintering it was observed that the lowest resistances for Approach 2 – NF:NW 60:40 samples were obtained after the samples were subjected to a pulse sequence of fluences 1 to 7 J/cm^2 respectively. Sample 1 had a resistance of 433 Ω/cm before IPL sintering. After adding the top PDMS layer its resistance rose to 450 Ω/cm. Sample 1 showed a decline in resistance upon IPL sintering with a sequence of increasing fluences. At 5 J/cm^2 it was at its lowest resistance of 376 Ω/cm. After IPL sintering, the sample was picked up from its mold during which it lost resistanc. Sample 2 started with an unsintered resistance of 500 Ω/cm. Its resistance increased to 519 Ω/cm after adding the top PDMS layer. Sample 2 showed a decrease in resistance upon IPL sintering too. At a fluence of 6 J/cm^2, Sample 2 showed its lowest resistance of 357 Ω/cm. Like the previous sample, Sample 2 also lost conductivity when it was picked up from its mold after sintering.

Table 6. IPL Fluence Sequence and Resistances for Approach 2 – NF:NW 80:20 samples

	SAMPLE 1	SAMPLE 2
IPL Fluence (J/cm^2)	Line Resistance (Ω/cm)	Line Resistance (Ω/cm)
0	433	500
After Top Layer	450	519
1	418	488
2	392	458
3	382	421
4	378	386
5	376	368
6	∞	357

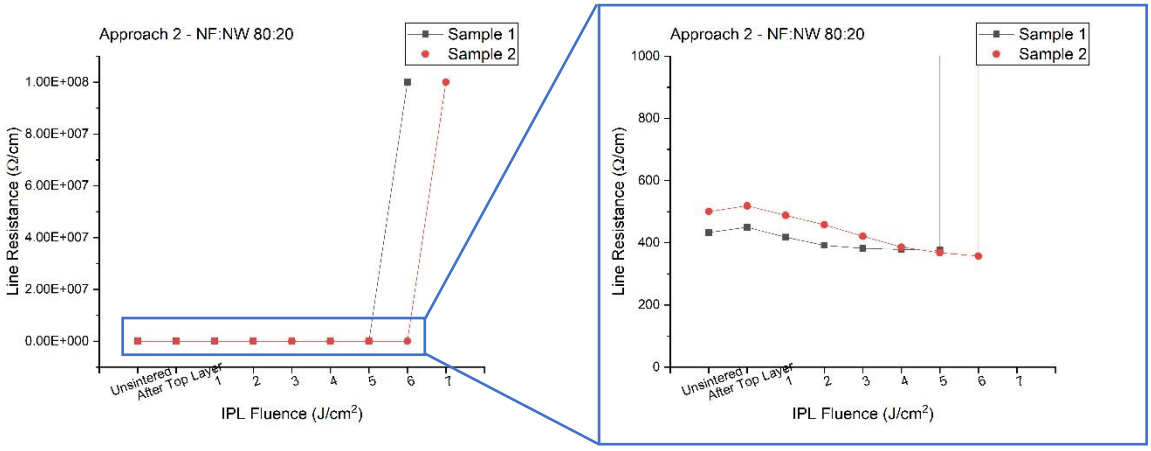

Fig 23. IPL – Resistance trends for Approach 2 – NF:NW 80:20 samples

Figure 23 shows the similar trend in reduction of resistance of Approach 2 – NF:NW 80:20 samples. It can be noted that addition of the top PDMS layer before IPL sintering enables the interconnects to endure greater fluences under IPL. The top layer acts as a protective cover. Unlike the NF:NW 80:20 samples in Approach 1, the Ag nanomaterial layer undergoes minimal damage during IPL sintering. There is no blow-off of the nanomaterial in Approach 2. However, the samples in Approach 2 – NF:NW 80:20 were still very sensitive and susceptible to mechanical damage as soon as they were picked up after sintering. Due to this, NF:NW 80:20 samples were bad candidates for bending.

3.4.2 NF:NW 60:40 ratio

Two samples of NF:NW 60:40 weight ratio have been documented for Approach 2. Upon IPL sintering it was observed that the lowest resistances for Approach 2 – NF:NW 60:40 samples were obtained after the samples were subjected to a pulse sequence of fluences 1 to 4 J/cm^2 respectively. Unlike the NF:NW 80:20 weight ratio samples in Approach 2, the NF:NW ratio samples showed very low resistances, both before and after IPL sintering, making this weight ratio and approach the most compatible combination for the

manufacture of the flexible interconnects in this research. The samples showed good bending behavior as well, as shown in Figures 25 and 26 below. Sample 1 showed a low unsintered resistance of 1.82 Ω/cm. Its resistance increased to 2.12 Ω/cm after adding the top PDMS layer. After an IPL pulse fluence sequence up to 4 J/cm^2, its resistance decreased to 1.58 Ω/cm. Sample 2 had an unsintered resistance of 2.09 Ω/cm, which increased to 2.64 Ω/cm after addition of the top PDMS layer. At a fluence of 4 J/cm^2, its resistance decreased to 1.90 Ω/cm.

Table 7. IPL Fluence Sequence and Resistances for Approach 2 – NF:NW 60:40 samples

	SAMPLE 1	SAMPLE 2
IPL Fluence (J/cm^2)	Line Resistance (Ω/cm)	Line Resistance (Ω/cm)
0	1.82	2.09
After Top Layer	2.12	2.64
1	2.08	2.51
2	1.84	2.13
3	1.82	2.06
4	1.58	1.90

Figure 24 shows the high similarity in resistance change for Samples 1 and 2 during IPL sintering. There is a small increase in resistance for both samples upon adding the top PDMS layer, after which their resistance reduces considerably. The resistance of both samples at a fluence of 4 J/cm^2 is considerably lower than their unsintered resistances.

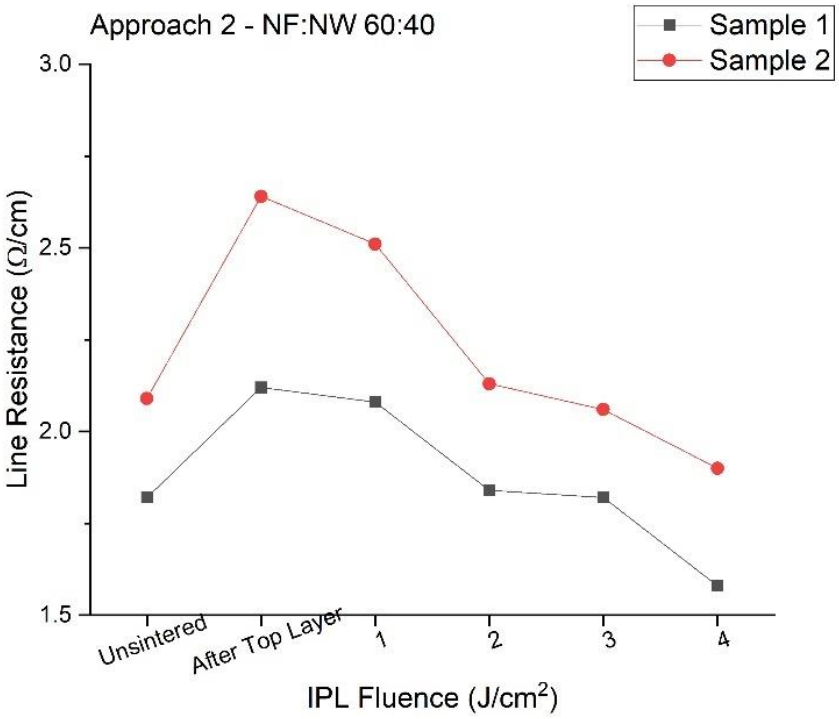

Fig 24. IPL – Resistance trends for Approach 2 – NF:NW 60:40 samples

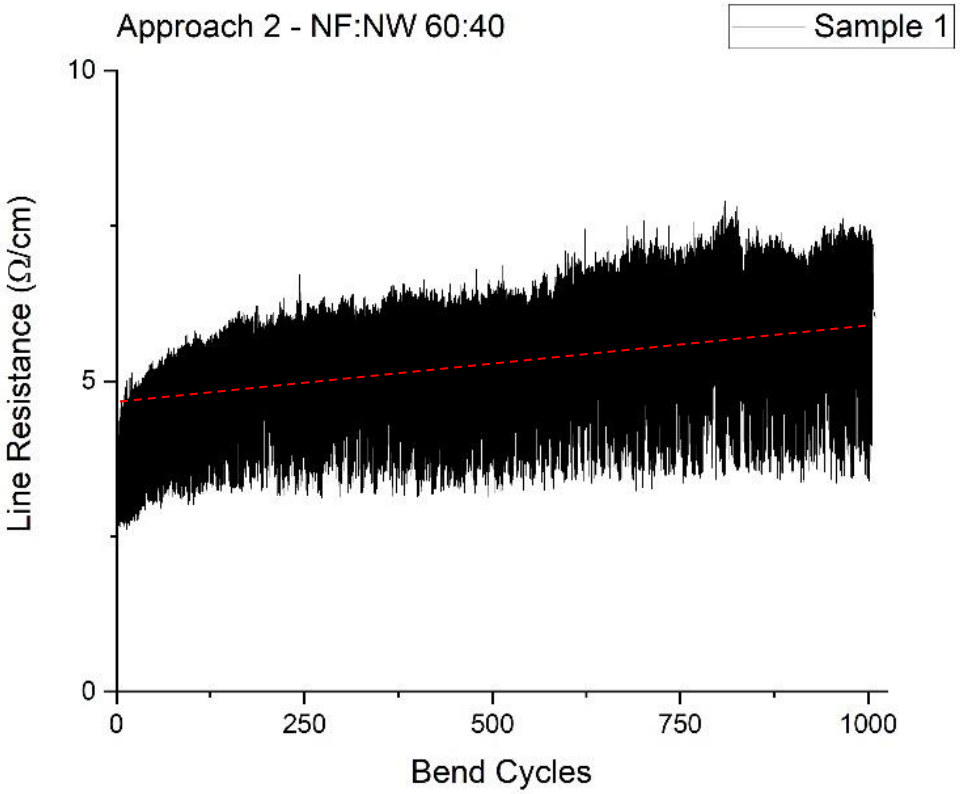

Fig 25. Dynamic hysteresis during bending for Approach 2 – NF:NW 60:40 Sample 1

Figure 25 shows the dynamic resistance hysteresis of Sample 1 during bending on the mechanical tester. Due to unavoidable mechanical resistance while the sample was picked up and placed for testing, the resistance right before bending was 2.12 Ω/cm. During bending, it can be noted that the resistance increases slightly for the first 100 bends after which it levels off around a resistance of 4.8 Ω/cm up to 1000 bend cycles. After bending, Sample 1 had a resistance of 3.9 Ω/cm when taken off the tester, and was still electrically conductive post-bending.

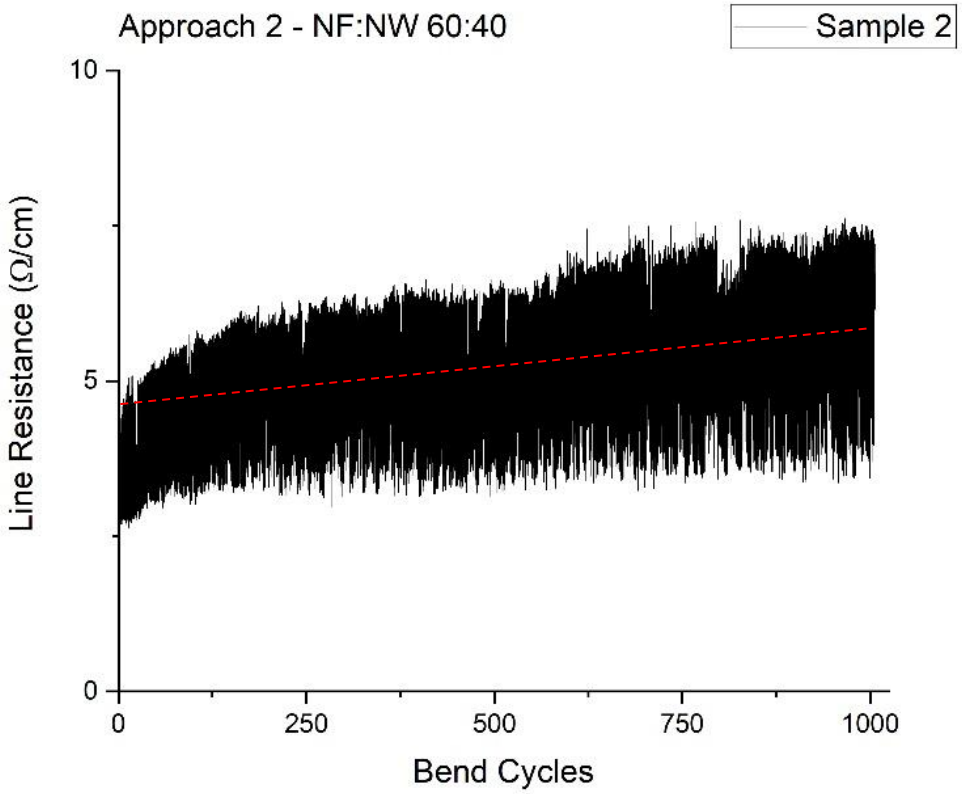

Fig 26. Dynamic hysteresis during bending for Approach 2 – NF:NW 60:40 Sample 2

Figure 26 shows the dynamic resistance hysteresis of Sample 2 during bending on the mechanical tester. Due to unavoidable mechanical resistance while the sample was picked

up and placed for testing, the resistance right before bending was 2.92 Ω/cm. During bending, it can be noted that the resistance increases slightly for the first 100 bends after which it levels off around a resistance of 4.9 Ω/cm up to 1000 bend cycles. After bending, Sample 2 had a resistance of 4.4 Ω/cm when taken off the tester, and was still electrically conductive post-bending.

3.4.3 NF:NW 40:60 ratio

Two samples of NF:NW 40:60 weight ratio have been documented for Approach 2. Upon IPL sintering it was observed that the lowest resistances for Approach 2 – NF:NW 40:60 samples were obtained after the samples were subjected to a pulse sequence of fluences 1 to 4 J/cm^2 respectively. The resistances of the samples in this case were comparable to the resistance of the NF:NW 60:40 ratio samples. Sample 1 had a resistance of 1.92 Ω/cm before sintering. After adding the top PDMS layer its resistance increased to 2.92 Ω/cm. After the IPL pulse fluence, its resistance dropped to 2.86 Ω/cm. Sample 2 had a resistance of 1.76 Ω/cm before sintering, which increased to 1.86 Ω/cm after addition of the top PDMS layer. At a fluence of 4 J/cm^2 its resistance dropped to 1.74 Ω/cm.

Table 8. IPL Fluence Sequence and Resistances for Approach 2 – NF:NW 40:60 samples

	SAMPLE 1	SAMPLE 2
IPL Fluence (J/cm^2)	Line Resistance (Ω/cm)	Line Resistance (Ω/cm)
0	1.92	1.76
After Top Layer	2.92	1.86
1	2.91	1.84
2	2.90	1.8
3	2.88	1.78
4	2.86	1.74

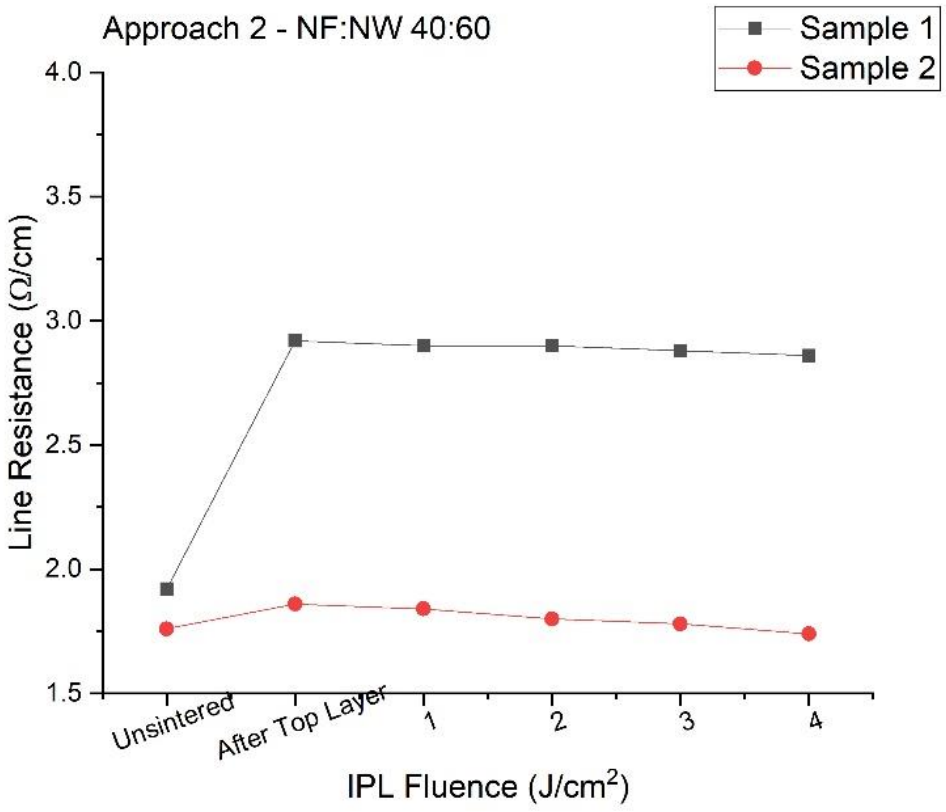

Fig 27. IPL – Resistance trends for Approach 2 – NF:NW 40:60 samples

Figure 27 shows the trend in resistance changes for Samples 1 and 2 during IPL. It can be observed that there were differences in the resistance change for both these samples after adding the top PDMS layer. While Sample 1 underwent a 1 Ω/cm increase in resistance after the top layer was added, the resistance of Sample 2 increased only by 0.1 Ω/cm. NF:NW 40:60 samples show a higher inconsistency in behavior as compared to NF:NW 60:40 weight ratio samples in both Approaches. This could be because Ag nanowires are more likely to get displaced, disfigured or damaged during the addition of the top PDMS layer leading to differences between the resistance and overall quality of the samples. Another important observation is that IPL sintering does not affect the resistance significantly. While Sample 2 shows a reduction in resistance of 0.12 Ω/cm, Sample 1

shows a reduction of only 0.06 Ω/cm. It is safe to say that Approach 2 – NF:NW 40:60 weight ratio samples do not benefit from the IPL sintering process.

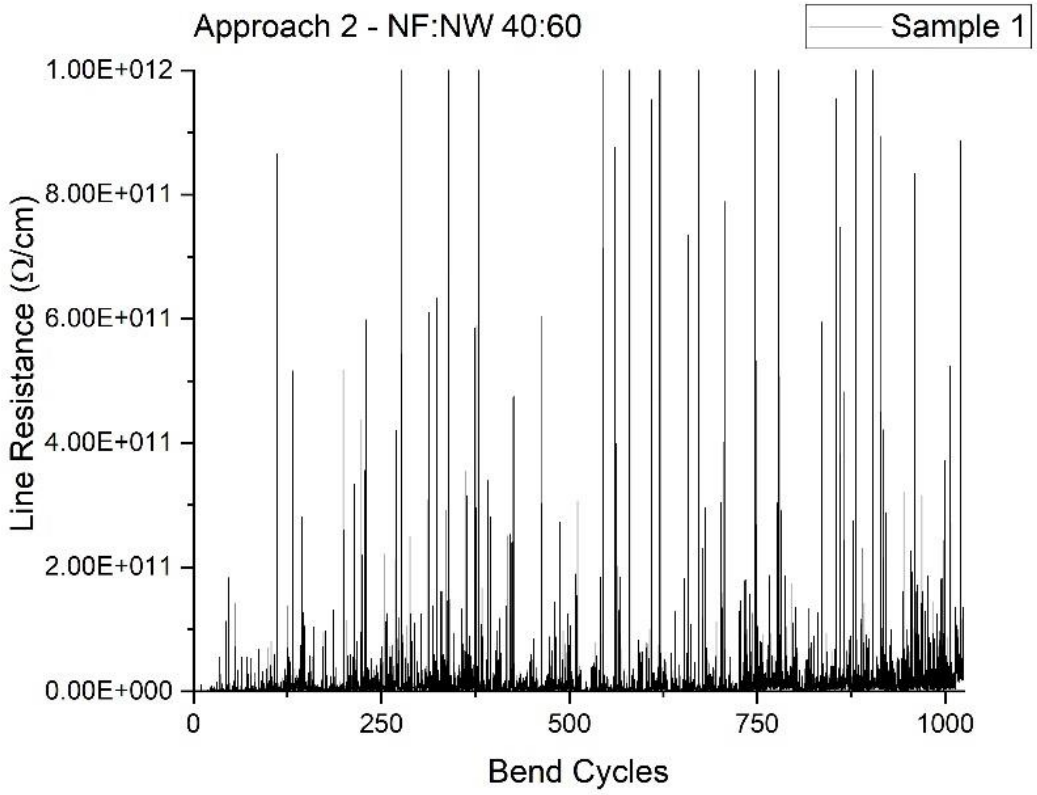

Fig 28. Dynamic hysteresis during bending for Approach 2 – NF:NW 40:60 Sample 1

Figure 28 and 29 show the dynamic resistance hysteresis of Samples 1 and 2 respectively during bending on the mechanical tester. Sample 1 had a resistance of 2.77 Ω/cm right before the bending process began, and Sample 2 had a resistance of 2.99 Ω/cm before bending. This increase in resistance took place during the removal of samples from their molds and setting them up in the bending tester.

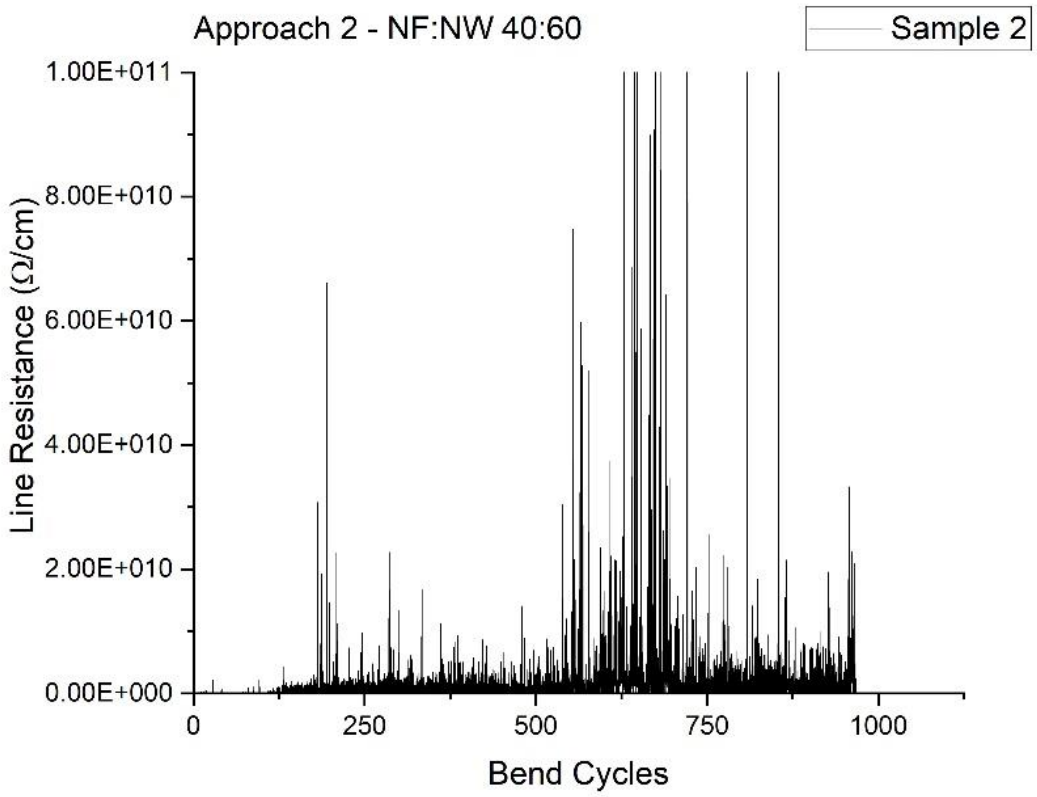

Fig 29. Dynamic hysteresis during bending for Approach 2 – NF:NW 40:60 Sample 2

It can be seen from the graphs that the resistances shoot up to the order of 10^{12} Ω/cm while in bent state. In unbent state, the samples showed a resistance in the order kilo Ω/cm. While this resistance is very high compared to the recorded resistances of the samples after IPL, it must be noted that the sample resistances were fairly uniform in their unbent-state resistances during bending. Both these samples survived 1000 bend cycles but lost electrical conductivity as soon as they were removed from the testing set-up. Based on these observations, it is inferred that these NF:NW 40:60 weight ratio samples were highly sensitive, during bending, unlike the samples in the NF:NW 60:40 ratio in the same

approach. However, these samples were also more susceptible to damage due to higher Ag nanowire content.

3.4.4 NF:NW 20:80 ratio

Two samples of NF:NW 20:80 weight ratio have been documented for Approach 2. Upon IPL sintering it was observed that the samples stayed conductive until a pulse fluence of 4 J/cm^2, beyond which the samples lost conductivity. The resistances of the samples in this case, in unsintered state, were comparable to the resistance of the NF:NW 60:40 ratio samples. Sample 1 showed a resistance of 3 Ω/cm before sintering. Upon adding the top PDMS layer, its resistance increased significantly to 10.2 Ω/cm. However, IPL sintering was counterproductive to the sample, as its resistance increased with increase in IPL fluence. At a fluence of 4 J/cm^2 its resistance rose to 120.2 Ω/cm which is considerably higher than its resistance before sintering. Following a similar trend, Sample 2 had a low resistance of 2.2 Ω/cm before sintering. Upon adding the top PDMS layer, its resistance was 7.6 Ω/cm. After sintering, its resistance increased to 114.8 Ω/cm at a fluence of 4 /cm^2.

Table 9. IPL Fluence Sequence and Resistances for Approach 2 – NF:NW 20:80 samples

	SAMPLE 1	SAMPLE 2
IPL Fluence (J/cm^2)	Line Resistance (Ω/cm)	Line Resistance (Ω/cm)
0	3	2.2
After Top Layer	10.2	7.6
1	26.6	30
2	45.8	56.6
3	76	73
4	120.2	114.8

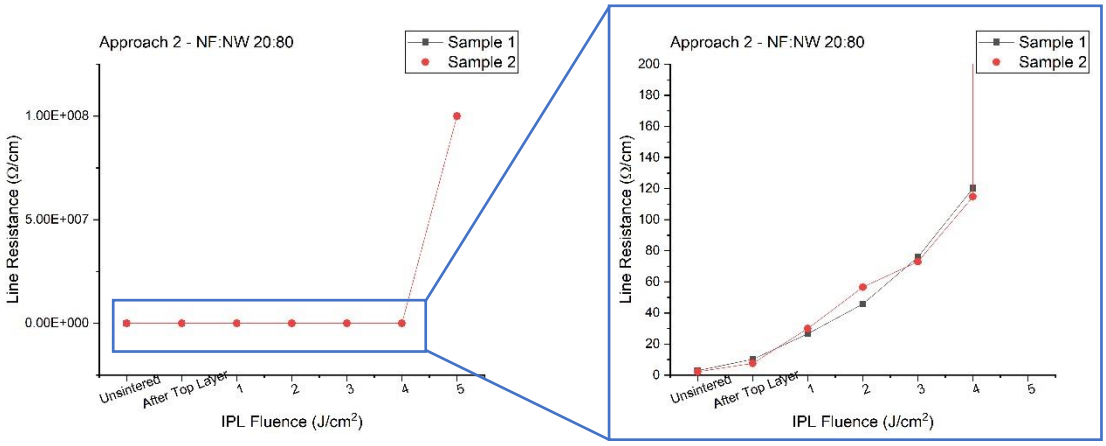

Fig 30. IPL – Resistance trends for Approach 2 – NF:NW 20:80 samples

Figure 30 shows the increase in resistance of Sample 1 and 2 with increase in IPL fluence. While both samples show similar behavior, the increase in resistance during sintering is a clear indication that IPL is detrimental to sample quality. Upon removing the samples from their molds, their resistances shot up to an order of Mega Ω/cm, making them bad candidates for bending testing.

3.5 Summary of Approach 2

Table 10: Variation in sample quality for Approach 1 samples

	NF:NW			
	80:20	**60:40**	**40:60**	**20:80**
Resistance before IPL				
Resistance after adding top PDMS layer				
Resistance after IPL				
Low resistance during bending				

	Good		Fair		Bad

1. Resistance of samples before IPL sintering: It was observed that Approach 2 samples of weight ratios NF:NW 60:40, 40:60 and 20:80 showed very low resistances before sintering. NF:NW 80:20 samples in this approach however showed higher resistances. As mentioned in the summary of Approach 1 samples, NF:NW 80:20 samples have high inconsistency in terms of AJP deposition. The observed difference in unsintered resistances can be explained on this basis.

2. Resistance of samples after adding top PDMS layer: It was seen in Approach 1 that adding the top PDMS layer would increase the resistance of the flexible interconnect samples. The same was observed in Approach 2 as well. However, it was also seen seen that samples with higher content of Ag nanoflake or nanowire suffered a greater increase

in resistance on adding the top layer, as compared to samples with similar nanoflake to nanowire concentration ratios.

3. Resistance of samples after IPL sintering: Samples in Approach 2 seem to be able to endure a longer sequence of pulses under IPL. This is because the top PDMS layer acts as a protective shielding, keeping the Ag nanomaterial in place and preventing blow off. NF:NW 60:40 samples both showed significantly lower resistances after IPL sintering. NF:NW 40:60 samples showed a slight decrease in resistance after IPL. However, IPL seemed to have a negative effect on NF:NW 20:80 weight ratio samples, as their resistance increased with increase in IPL fluence. Observing the differences in resistance before and after sintering for the 4 weight ratios, it can be inferred that the reduction in resistance during IPL is inversely proportional to the amount of Ag nanoflakes in the samples. While samples with NF:NW 80:20 ratio showed a 70 – 150 Ω/cm reduction in resistance after IPL sintering, NF:NW 20:80 samples showed an increase in resistance by approximately 100 Ω/cm.

4. Low resistance during bending: A good quality flexible interconnect should have low resistance even when deformed. This implies that the resistance of the samples should have been as low as possible during the 1000 bending cycles. Out of the 4 weight ratios, only the NF:NW 60:40 and 40:60 samples were good candidates for bending. Out of these two, only the NF:NW 60:40 weight ratio samples showed low resistances during bending. They were also the only samples that stayed conductive even after 1000 bending cycles.

3.6 SEM Images

Sections 3.2 to 3.5 show that Approach 2 – NF:NW 60:40 weight ratio is the optimal fabrication route for the manufacture of flexible interconnects. To find out why this configuration is better than others, Scanning Electron Microscopy was done on the samples before IPL, after IPL and after bending. Cross-sections of the interconnects were studied to examine the effect of nanoflake-nanowire ratio on static and dynamic performance of the interconnects.

To prepare the samples for SEM, a 2 mm wide strip was cut from the interconnect and mounted on the sample holder. The strip was mounted such that the cut cross section was on top, as shown in Figure 31. This cross section had an exposed Ag nanomaterial layer, which was observed in SEM. The base of the sample was coated with a drop of Silver paint to ground the sample and avoid charge accumulation. Then, the sample was sputtered with a 10 nm layer of Gold. The instrument used was the Zeiss Sigma Field Emission Scanning Electron Microscope. Images were taken at an accelerating voltage (EHT) of 15kV, at magnifications ranging from 10K X to 50K X.

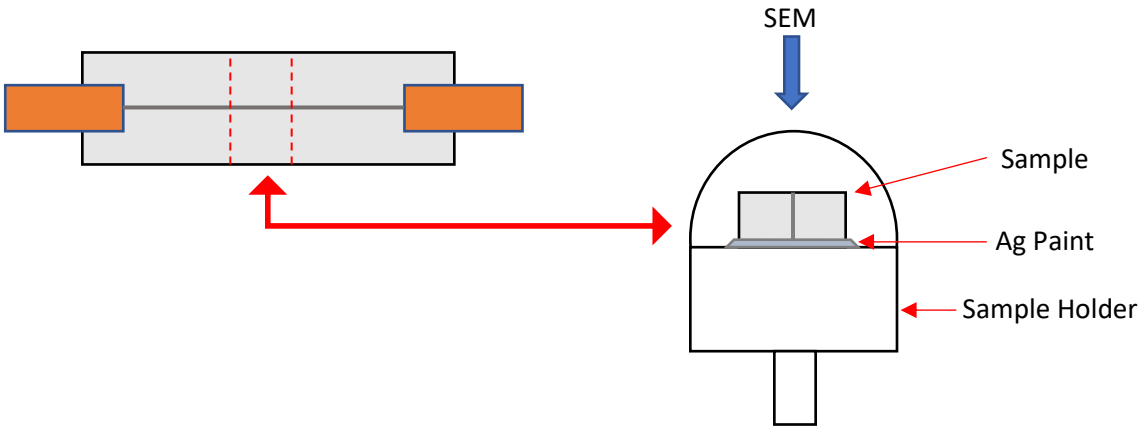

Fig 31. Schematic of sample orientation during SEM

3.6.1 SEM on NF:NW 60:40 samples

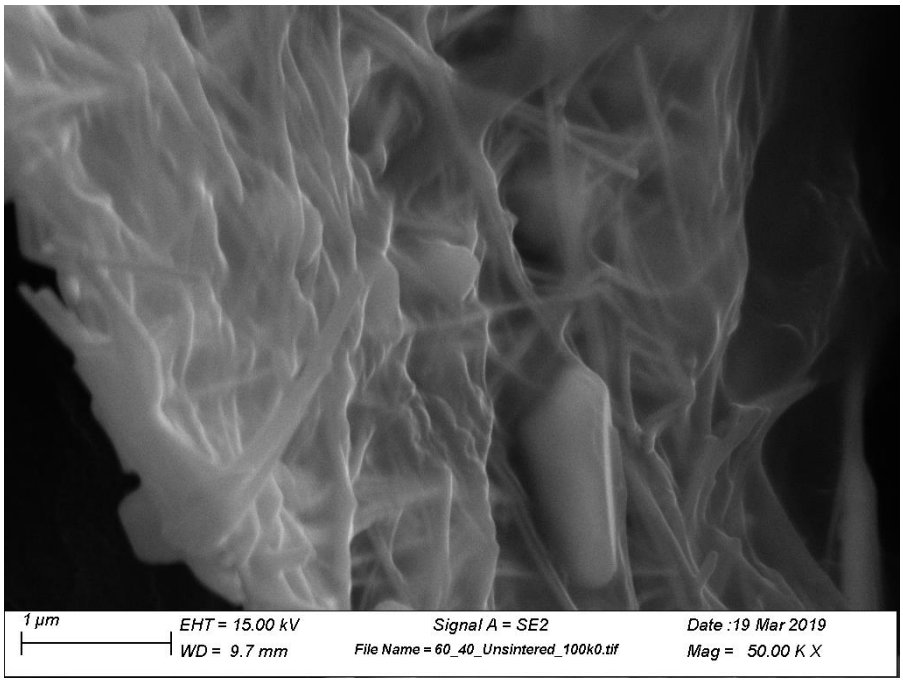

(a) Before IPL sintering (50K X magnification)

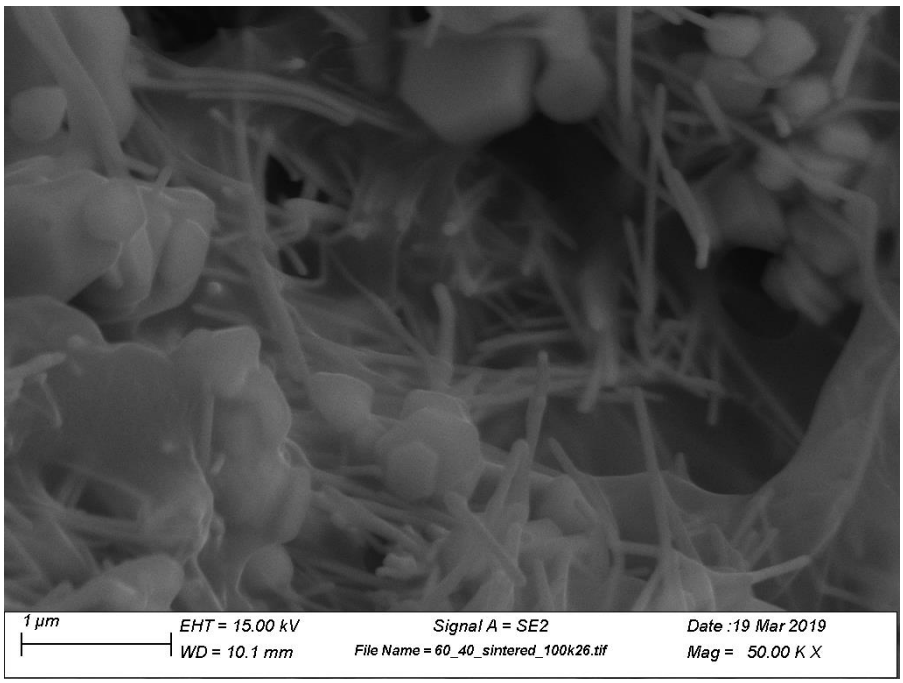

(b) After IPL sintering (50K X magnification)

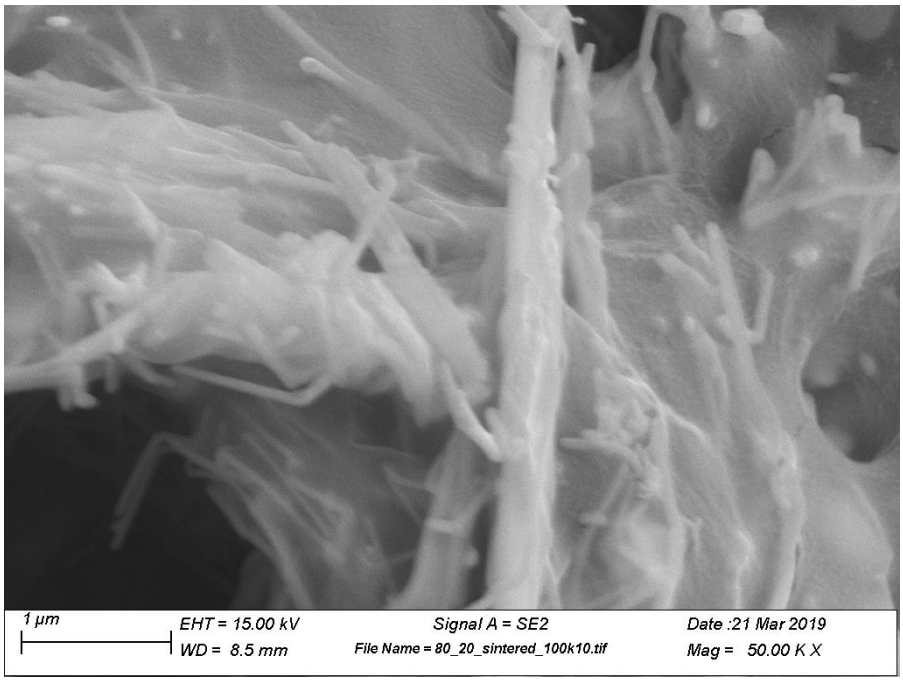

(c) After 1000 bending cycles (50K X magnification)

Fig 32. SEM Images of NF:NW 60:40 sample

3.6.2 SEM on NF:NW 40:60 samples

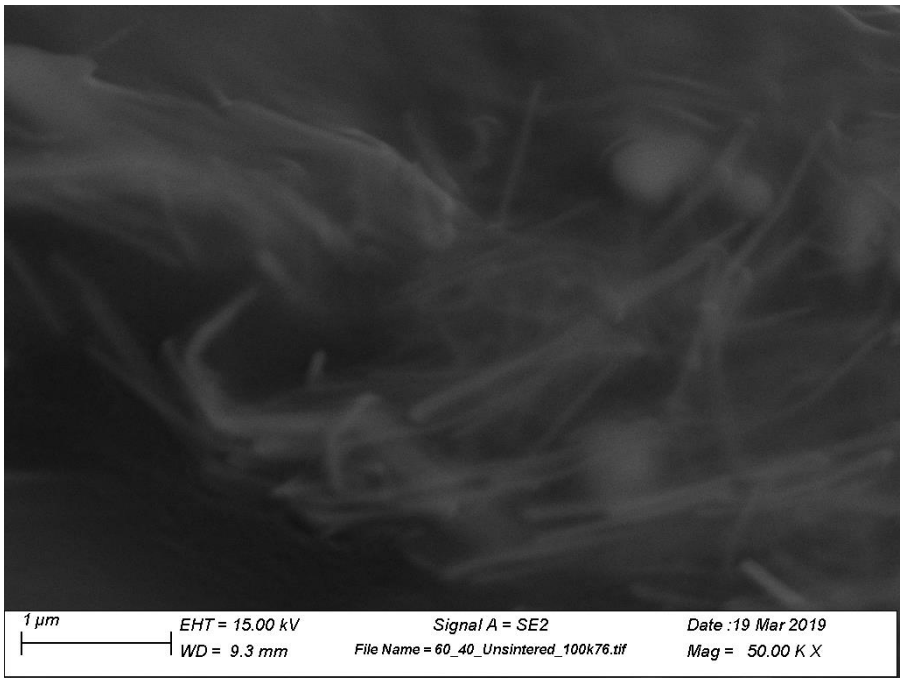

(a) Before IPL sintering (50K X magnification)

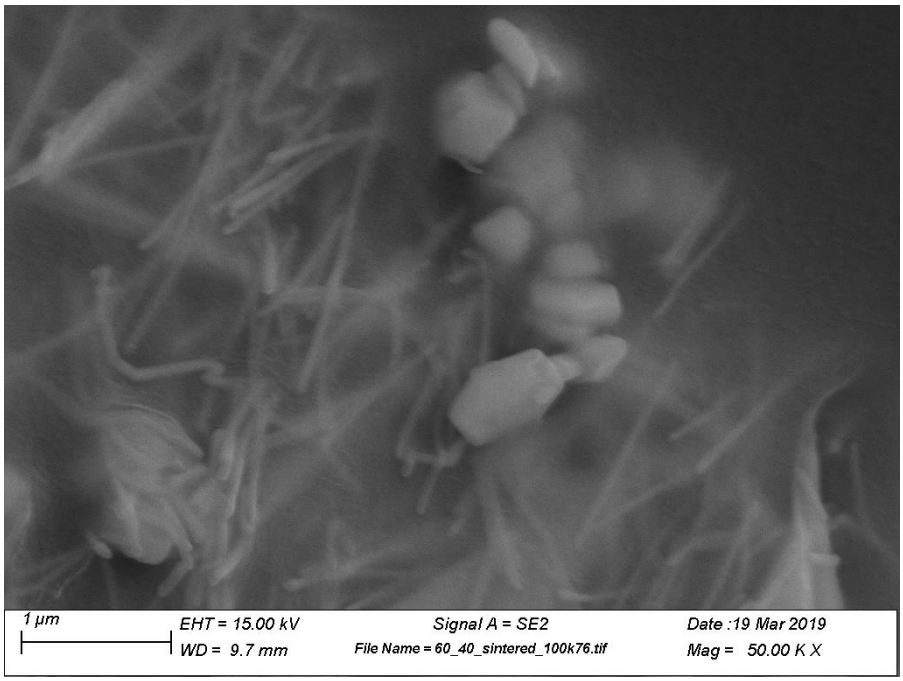

(b) After IPL sintering (50K X magnification)

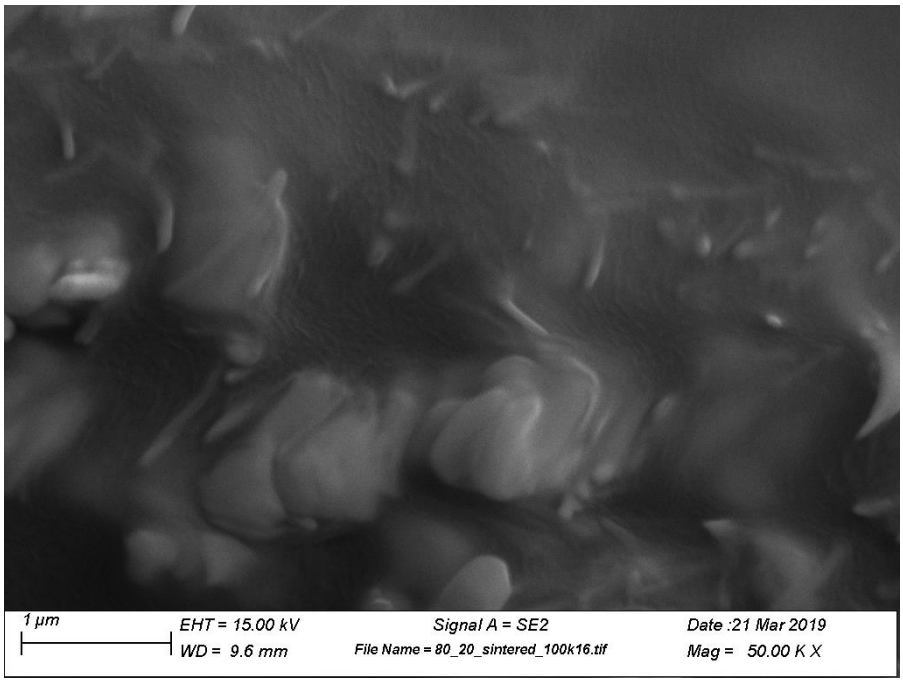

(c) After 1000 bending cycles (50K X magnification)

Fig 33. SEM Images of NF:NW 40:60 sample

Figures 32 and 33 show SEM images of the NF:NW 60:40 and NF:NW 40:60 ratio samples from Approach 2 respectively, describing the Ag nanomaterial before IPL sintering (a), after IPL sintering (b) and after 1000 bending cycles (c)

The SEM images show the fusing of nanomaterial after IPL, and the damage to nanomaterial after bending, up to a certain extent. However, there is no conclusive evidence of how the change in the nanomaterial affects the resistivity of the interconnect.

3.6.3 Ag nanomaterial layer thickness:

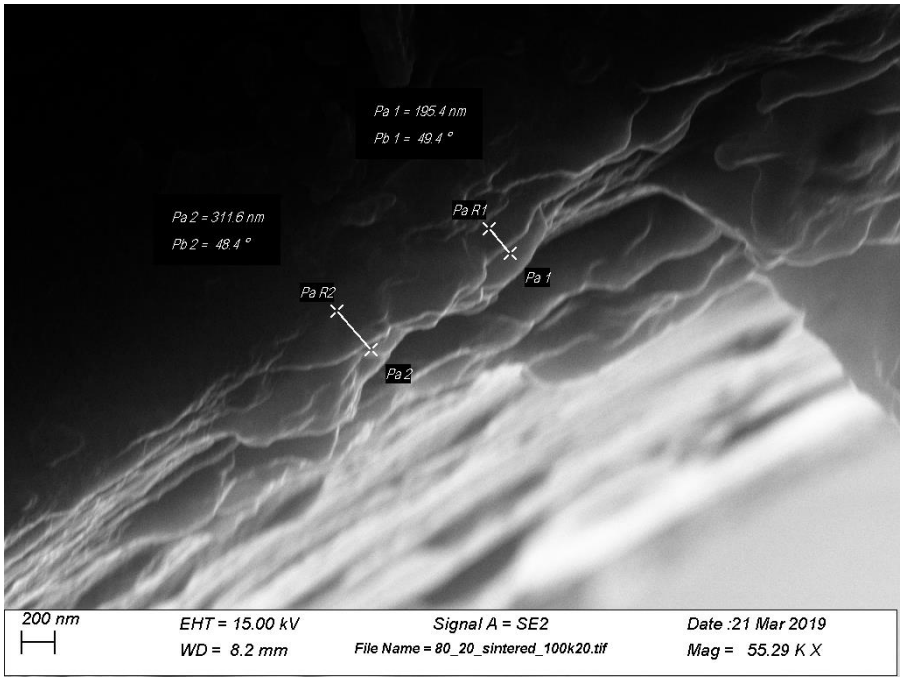

(a) NF:NW 60:40 sample

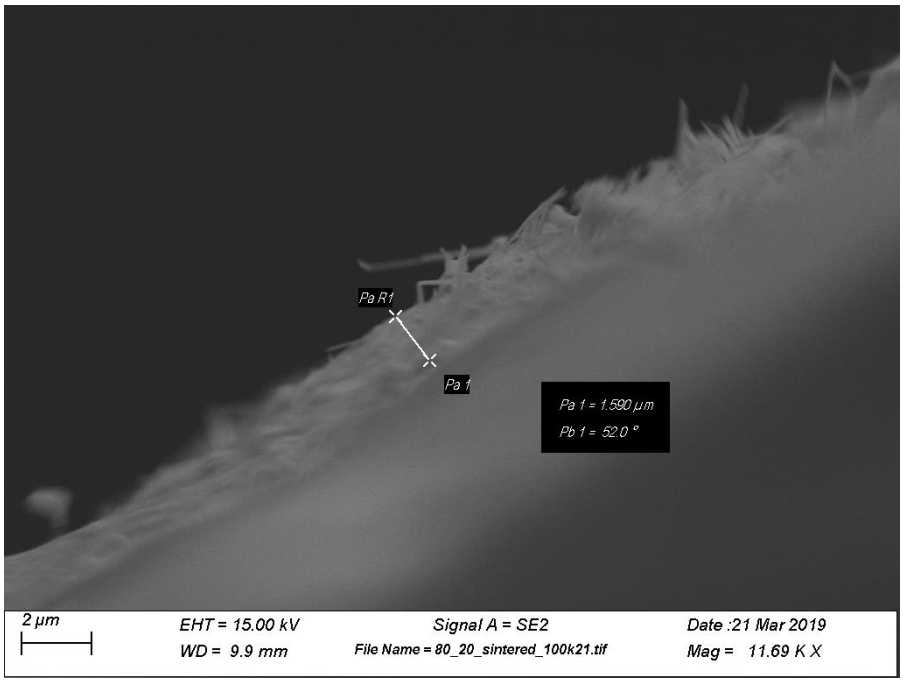

(b) NF:NW 40:60 sample

Fig 34. Ag nanomaterial layer thickness measurements

Due to the presence of PDMS over the nanomaterial in the Approach 2 samples, it was difficult to determine the thickness of the Ag layer deposited onto the sample. To measure the thickness of the Ag nanomaterial layer, samples of NF:NW 60:40 and NF:NW 40:60 ratio from Approach 1 were examined via SEM. These samples did not have an over-molded PDMS layer, making the nanomaterial clearly visible.

Figure 34 (a) shows the thickness measurement done on the Approach 1 - NF:NW 60:40 sample. It was observed that the nanomaterial layer varied between thicknesses of 190 nm to 320 nm throughout the sample. This layer was more uniform and consistent over the length of the sample. The nanomaterial layer in the NF:NW 60:40 samples was estimated to be an average value of 250 nm based on these readings.

Figure 34 (b) shows the thickness measurement done on the Approach 1 – NF:NW 40:60 sample. The nanomaterial layer had a uniform thickness of approximately 1.6 µm over the length of the sample. It must be noted that the difference in the thicknesses of the nanomaterial layer can be attributed to the difference in size of the Ag nanoflakes and nanowires, and the difference in the weight ratios. The nanoflakes have an in-plane size of 200-300 nm and a thickness of 20-30 nm. The nanowires have a diameter of 100 nm. Due to this, the Ag layer in the NF:NW 60:40 samples (having a greater quantity of nanoflakes) is more compact, as compared to the NF:NW 40:60 samples.

Using these thicknesses, the line resistance measurements on the NF:NW 60:40 and NF:NW 40:60 samples was converted to resistivity, as shown in Table 11.

Table 11. Resistivity of NF:NW 60:40 and NF:NW 40:60 samples

	NF:NW 60:40		NF:NW 40:60	
	SAMPLE 1	SAMPLE 2	SAMPLE 1	SAMPLE 2
	Resistivity (μΩ-cm)	Resistivity (μΩ-cm)	Resistivity (μΩ-cm)	Resistivity (μΩ-cm)
IPL Fluence				
0 J/cm^2	4.550	5.225	30.528	27.984
After Top Layer	5.300	6.600	46.428	29.574
1 J/cm^2	5.200	6.275	46.269	29.256
2 J/cm^2	4.600	5.325	46.110	28.620
3 J/cm^2	4.550	5.15	45.792	28.302
4 J/cm^2	3.950	4.750	45.474	27.666
Before bending	5.300	7.300	44.043	47.541
Avg. Resistivity during bending	12	12.25	(Inconsistent readings of the order 10^{11} Ohm/cm)	(Inconsistent readings of the order 10^{11} Ohm/cm)
After bending	9.750	11	∞	∞

The graphs for resistivity during bending of the Approach 2 – 60:40 samples are as shown in Figures 35 and 36.

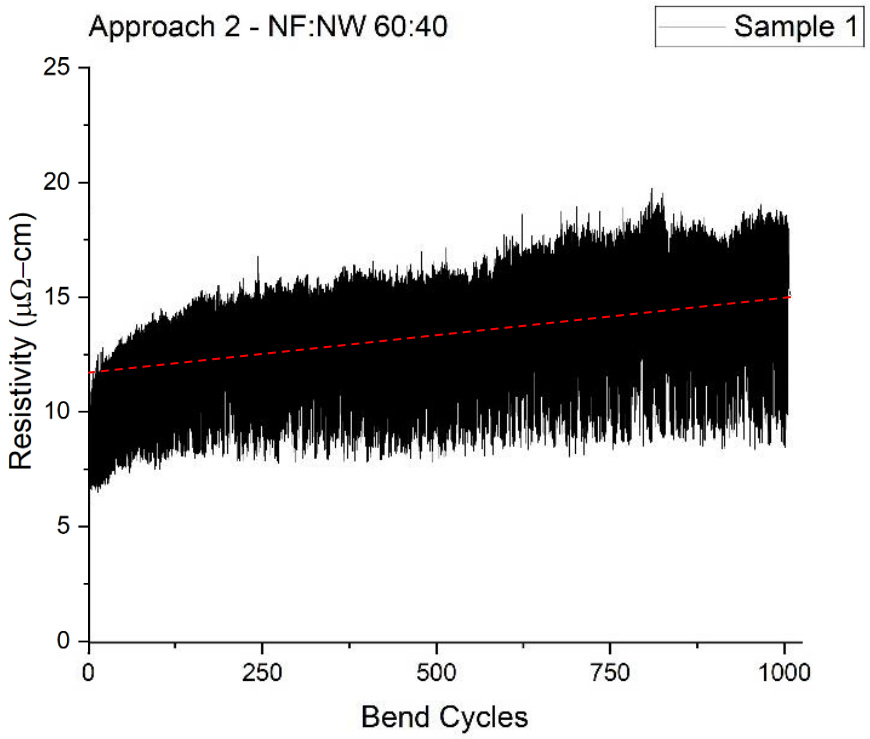

Fig 35. Resistivity hysteresis during bending of Approach 2 – NF:NW 60:40 S ample 1

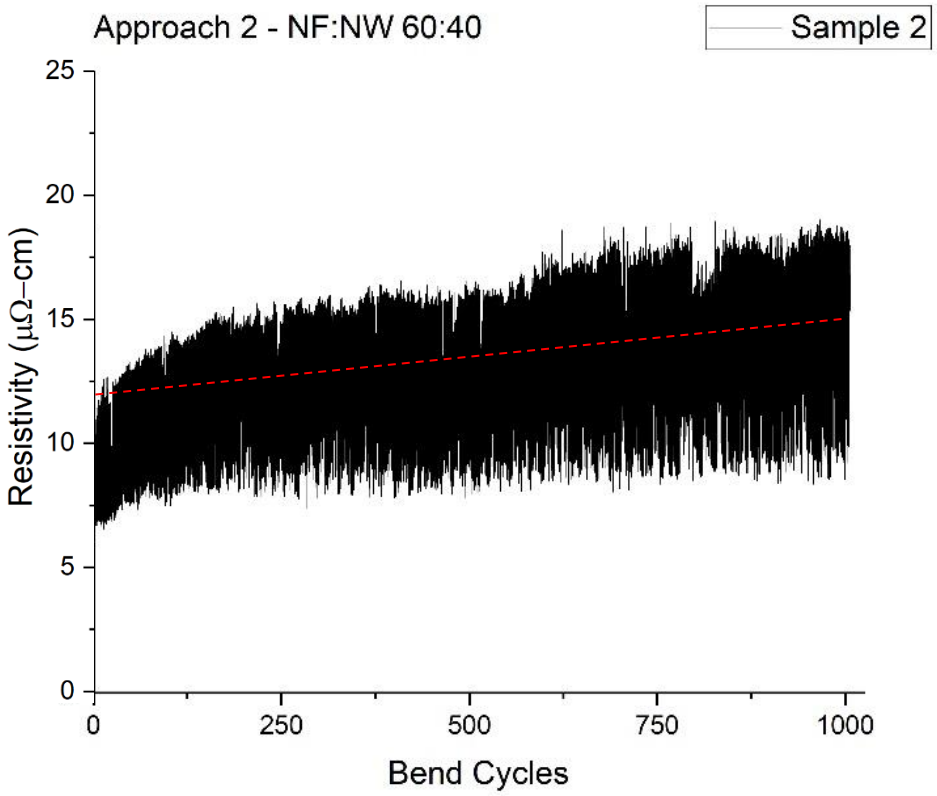

Fig 36. Resistivity hysteresis during bending of Approach 2 – NF:NW 60:40 Sample 2

Chapter 4

Conclusion

The flexible interconnects manufactured in this research follow two approaches, with four Ag nanoflake-nanowire ratios in each. It was observed that the Ag NF:NW 60:40 weight ratio in Approach 2 (IPL sintering after addition of top PDMS layer) shows best results. The samples in this configuration demonstrate very low resistance before deformation. These samples have a resistivity of approximately 4.8875 ± 0.3375 μΩ-cm before sintering. After IPL, their resistivity drops to around 4.35 ± 0.4 μΩ-cm. The samples also show very good behavior during bending. The resistance of the samples increases from 6.3 ± 1 μΩ-cm before bending to 10.375 ± 0.625 μΩ-cm after 1000 bend cycles. Further, the resistance trend is fairly linear and horizontal throughout the bending process after the initial break-in period.

It was observed over the course of this study that IPL sintering of samples yielded better results when it was done after adding the top PDMS layer on the samples. Sintering the Ag nanomaterial before encasing it in PDMS leads to a variety of problems such as damage to the nanomaterial under IPL and higher tendency of mechanical damage before bending. On the other hand, sintering after adding the top layer avoids these issues almost completely.

It was also observed that Ag NF:NW 60:40 weight ratio is the most optimal ratio for the manufacture of these interconnects. Weight ratios with higher percentage of nanoflake or nanowire do not adhere well to PDMS substrates. They also show high inconsistency of deposition during AJP sintering. Additionally, samples with higher Ag nanowire

concentration undergo detrimental effects under IPL sintering, as their resistance increases with increase in pulse fluence. The Ag NF:NW 40:60 ratio shows samples that have erratic fluctuations in resistance when bent. However, their resistances are fairly consistent when released, during the bending testing. This implies that there may be other NF:NW ratios between the 60:40 and 40:60 range which may yield good results.

This research is compared against 4 other research papers (mentioned in Chapter 1). The table below shows a comparison between the best results obtained in this research (Approach 2 – Ag NF:NW 60:40 samples) and the results obtained in these papers.

The criteria for comparison are the 3 goals of this research as stated in the scope of this research, namely:

1. Resistivity of the (processed) interconnect in static condition (R)

2. Change in resistivity of the sample during deformation (ΔR)

3. Electrical Hysteresis of the sample after 1000 bend cycles (ΔR')

Table 12. Comparison of results

Reference	26	29	30	31	This Research
Author	**Han et. al.**	**Shankar et. al.**	**Kim et. al.**	**Muth et. al.**	
Nanomaterial	Cu NW	Ag NP	Ag NF:NP	Carbon NP	Ag NF:NW
Transfer Process	Vacuum Filtration	Screen Printing	Embedding inside liquid elastomer	Embedded 3D Printing	AJP
Processing Method	Plasmonic Laser Sintering	IPL	IPL	None	IPL

Cyclic Deformation type	Folding (1500 folds)	Tensile strain (1 cycle)	Tensile strain (10000 cycles)	Tensile strain (5 cycles)	Bending around 5 mm radius (1000 cycles)
Resistivity of Unprocessed Sample	$10^3 – 10^9$ Ω/sq	42000 μΩ-cm	Not documented	11 kΩ	4.89 ± 0.33 μΩ-cm (Before top layer) 5.95 ± 0.65 μΩ-cm (After top layer)
	(Sheet Res.)			(Resistance)	
Resistivity of Processed Sample (R)	20 Ω/sq	15000 μΩ-cm	349.5 μΩ-cm	No processing done	4.35 ± 0.4 μΩ-cm (Before bending) 8.7 ± 0.4 μΩ-cm (After break-in period)
	(Sheet Res.)				
Resistivity Change During Deformation (ΔR)	~5 Ω/sq	~12 x 10^4 μΩ-cm	~174 μΩ-cm	~14.8 kΩ	8.385 ± 0.09 μΩ-cm (After break-in period)
Electrical Hysteresis after Cyclic Loading (ΔR')	4 Ω/sq	-	239 μΩ-cm	1.1 kΩ	1.675 ± 0.225 μΩ-cm (After break-in period)
Issues	Thickness of deposited Copper nanomaterial layer is not specified	No issues	Resistance of sample before IPL sintering is not specified	Geometry of printed interconnect is not specified	-

4.1 Future Work:

As seen from above results, this study has demonstrated a new method to produce flexible interconnects with low resistance and good performance under repeated deformation. However, there is further scope of improvement in this field, described below:

1. Testing of other NF:NW ratios: This research establishes that Approach 2 - Ag NF:NW 60:40 weight ratio is the optimal approach for manufacture of flexible interconnects. It also goes on to show that Ag NF:NW 40:60 ratio samples shows poor consistency in bent state resistance. All weight ratios apart from these two do not show any result in cyclic bending. This implies that there may be other NF:NW ratios between the 60:40 – 40:60 region which may show promising results. By adjusting the weight ratios of Ag nanoflake and nanowire in this region, it may be possible to strike an even better balance between low resistance and high sensitivity.

2. Different cyclic deformation tests: Flexible interconnects are often subject to deformation in the form of stretching, bending and torsion. In this research, the dynamic resistance behavior of samples is characterized only by bending. However, the samples can also be tested for performance in tensile strain and torsion. The elastomer PDMS used in this study is prepared and cured as per standard manufacturing procedures i.e. 10 parts by weight of polymer is mixed with 1 part by weight of curing agent, and cured at room temperature. However, it is possible to increase the elasticity of PDMS samples by reducing the quantity of curing agent. Using this approach, the interconnects can be made more elastic, and their performance can be tested under torsion and tensile strain.

3. Re-sintering: Due to mechanical damage to the Ag nanomaterial during bending, its resistance increases. It was observed during this research, that sintering the sample via IPL after bending can reduce its resistance once again. This re-sintered sample was bent again for 1000 bends.

Sample 1 from Approach 2 – NF:NW 60:40 shown above was used to demonstrate performance after re-sintering. As demonstrated in Chapter 3, this sample endured 1000 bending cycles on the tester without loss of conductivity. After being taken off the tester, this sample was subjected to IPL sintering again. Table 13 and Figure 37 show the IPL pulse sequence and resistance change in the sample during IPL.

Table 13. IPL Fluence Sequence and Resistances for Re-sintered Approach 2 – NF:NW 60:40 samples.

	SAMPLE 1
IPL Fluence (J/cm^2)	Line Resistance (Ω/cm)
0	3.9
1	2.72
2	2.8
3	2.76
4	2.34
5	2.24
6	2.07
7	3.36

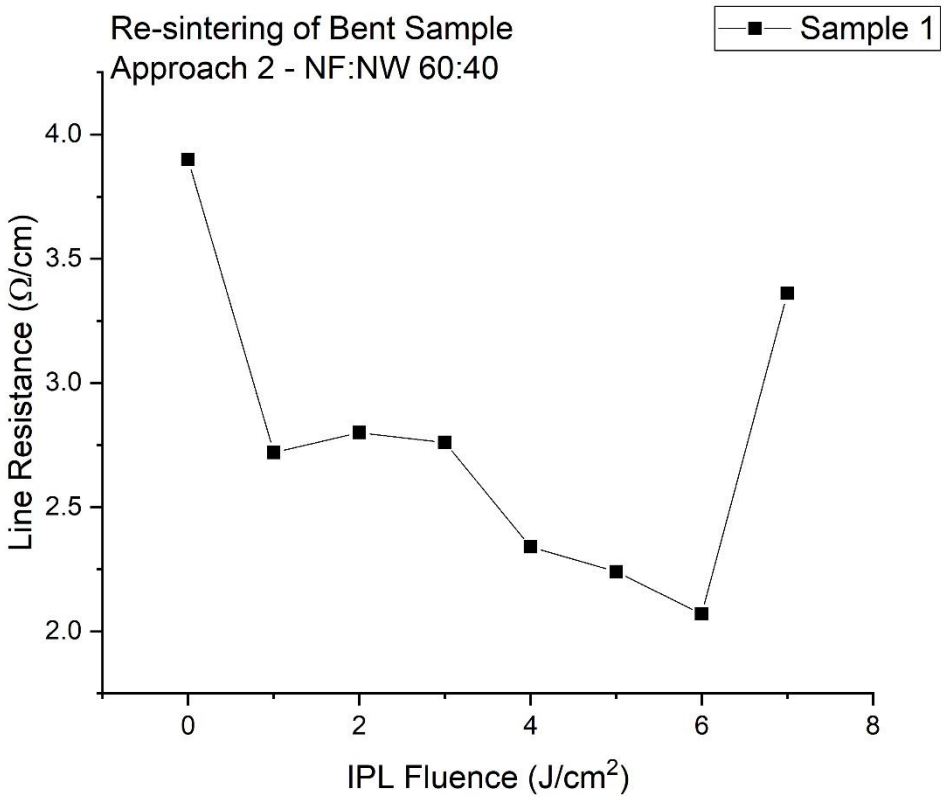

Fig 37. IPL – Resistance trend for Re-sintered Approach 2 – NF:NW 60:40 Sample 1

Figure 37 shows that sintering the interconnect via IPL, after the sample was subjected to bending, reduces its resistance once again. The sample showed the lowest resistance of 2.07 Ω/cm upon re-sintering, which was similar to the resistance obtained upon sintering the sample for the first time (1.58 Ω/cm). It can be noted that the sample had to be sintered to a fluence of 6 J/cm^2 to obtain this resistance, while the sample was sintered up to 4 J/cm^2 the first time. This sample was subjected to another 1000 cycles of bending. The results obtained can be seen in Figure 38 below.

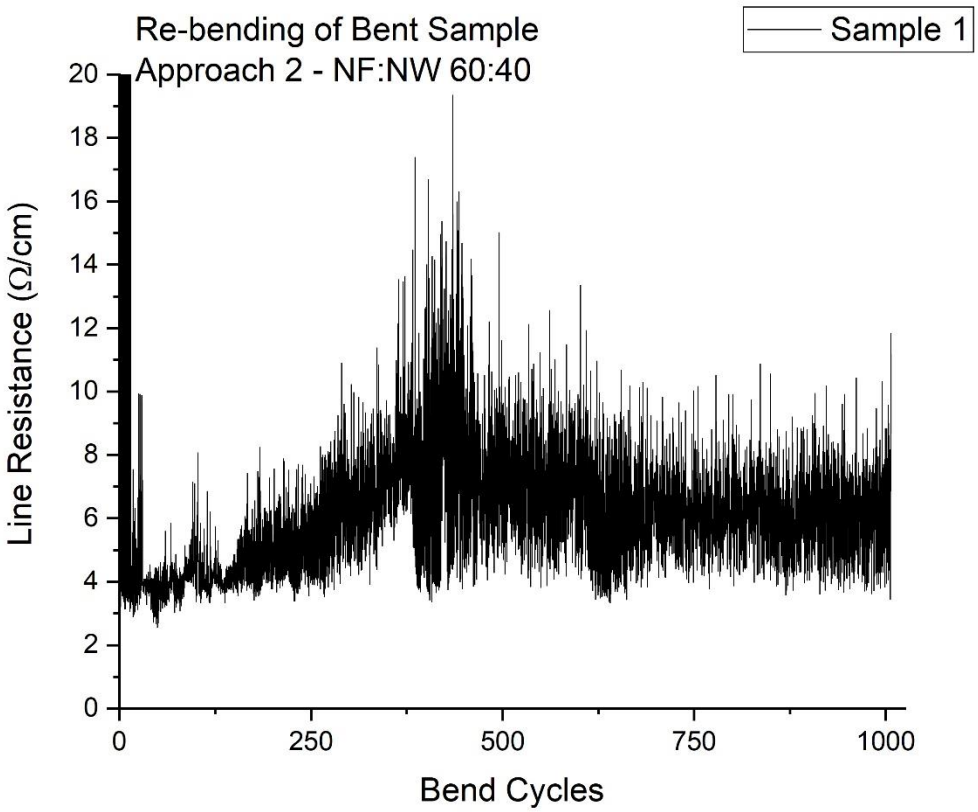

Fig 38. Dynamic hysteresis during re-bending of re-sintered Approach 2 – NF:NW 60:40 Sample 1

It can be seen that the sample showed very inconsistent resistance over the course of bending. The resistance of the sample in bent state as well as un-bent state were highly non-uniform for the first 450 bends, after which they stabilized to a certain extent around an average value of 7 Ω/cm. This sample stayed conductive even after being taken off the tester after the second iteration of bending.

The results obtained showed that the sample survives the bending cycles but shows inconsistent resistance. However, it can be inferred from this case that re-sintering seems to repair the interconnect by once again fusing some of the nanomaterial that had

undergone damage during bending. This phenomenon can be studied, to determine the repairability of the flexible interconnects.

References

1. Alexander Kamyshny, Shlomo Magdassi. Conductive Nanomaterials for Printed Electronics. *Small*, 10 (17): 3515-3535, 2014.

2. Takeo Yamada, Yuhei Hayamizu, Yuki Yamamoto, Yoshiki Yomogida, Ali Izadi-Najafabadi, Don N. Futaba, Kenji Hata. A stretchable carbon nanotube strain sensor for human-motion detection. *Nature Nanotechnology*, 6: 296-301, 2011.

3. Yan Wang, Li Wang, Tingting Yang, Xiao Li, Xiaobei Zang, Miao Zhu, Kunlin Wang, Dehai Wu, Hongwei Zhu. Wearable and Highly Sensitive Graphene Strain Sensors for Human Motion Monitoring. *Advanced Functional Materials*, 24: 4666-4670, 2014.

4. Morteza Amjadi, Aekachan Pichitpajongkit, Sangjun Lee, Seunghwa Ryu, Inkyu Park. Highly Stretchable and Sensitive Strain Sensor Based on Silver Nanowire-Elastomer Nanocomposite. *ACS Nano*, 8(5): 5154-5163, 2014.

5. R. J. N. Helmer, D. Farrow, K. Ball, E. Phillips, A. Farouil, I. Blanchonette. A pilot evaluation of an electronic textile for lower limb monitoring and interactive biofeedback. *ScienceDirect Procedia Engineering*, 13, 513-518, 2011.

6. Joseph T. Muth, Daniel M. Vogt, Ryan L. Truby, Yig˘it Mengüç, David B. Kolesky, Robert J. Wood, Jennifer A. Lewis. Embedded 3D Printing of Strain Sensors within Highly Stretchable Elastomers. *Advanced Materials*, 26, 6307-6312, 2014.

7. Dae-Hyeong Kim, Nanshu Lu, Rui Ma, Yun-Soung Kim, Rak-Hwan Kim, Shuodao Wang, Jian Wu, Sang Min Won, Hu Tao, Ahmad Islam, Ki Jun Yu, Tae-il Kim, Raeed Chowdhury, Ming Ying, Lizhi Xu, Ming Li, Hyun-Joong Chung, Hohyeun Keum, Martin McCormick, Ping Liu, Yong-Wei Zhang, Fiorenzo G. Omenetto, Yonggang Huang, Todd Coleman, John A. Rogers. Epidermal Electronics. *Science*, 333, 838-844, 2011.

8. Changhyun Pang, Gil-Yong Lee, Tae-il Kim, Sang Moon Kim, Hong Nam Kim, Sung-Hoon Ahn, Kahp-Yang Suh. A flexible and highly sensitive strain-gauge sensor using reversible interlocking nanofibres. *Nature Materials*, 11, 795-801, 2012.

9. Nanshu Lu, Chi Lu, Shixuan Yang, John Rogers. Highly Sensitive Skin-Mountable Strain Gauges Based Entirely on Elastomers. *Advanced Functional Materials*, 22, 4044-4051, 2012.

10. Dae-Hyong Kim, Yun-Soung Kim, Jian Wu, Zhuangjian Liu, Jizhou Song, Hoon-Sik Kim, Yonggang Y. Huang, Keh-Chih Hwang, John A. Rogers. Ultrathin Silicon

Circuits With Strain-Isolation Layers and Mesh Layouts for High-Performance Electronics on Fabric, Vinyl, Leather and Paper. *Advanced Materials*, 21 (36), 3703-3707, 2009.

11. Sheng Xu, Yihui Zhang, Lin Jia, Kyle E. Mathewson, Kyung-In Jang, Jeonghyun Kim, Haoran Fu, Xian Huang, Pranav Chava, Renhan Wang, Sanat Bhole, Lizhe Wang, Yoon Joo Na, Yue Guan, Matthew Flavin, Zheshen Han, Yonggang Huang, John A. Rogers. Soft Microfluidic Assemblies of Sensors, Circuits and Radios for the Skin. *Science*, 344, 70-74, 2014.

12. Heung Cho Ko, Mark P. Stoykovich, Jizhou Song, Viktor Malyarchuk, Won Mook Choi, Chang-Jae Yu, Joseph B. Geddes III, Jianliang Xiao, Shuodao Wang, Yonggang Huang, John A. Rogers. A hemispherical electronic eye camera based on compressible silicon optoelectronics. *Nature*, 454, 748-753, 2008.

13. Dae-Hyeong Kim, Roozbeh Ghaffari, Nanshu Lu, John A. Rogers. Flexible and Stretchable Electronics for Biointegrated Devices. *Annual Review of Biomedical Engineering*, 14, 113-128, 2012.

14. Alessandro Levi, Matteo Piovanelli, Silvano Furlan, Barbara Mazzolai, Lucia Beccai. Soft, Transparent Electronic Skin for Distributed and Multiple Pressure Sensing. *Sensors*, 13, 6578-6604, 2013.

15. Ramses V. Martinez, Jamie L. Branch, Carina R. Fish, Lihua Jin, Robert F. Shepherd, Rui M. D. Nunes, Zhigang Suo, George M. Whitesides. Robotic Tentacles with Three-Dimensional Mobility Based on Flexible Elastomers. *Advanced Materials*, 25, 205-212, 2013.

16. Robert F. Shepherd, Filip Ilievski, Wonjae Choi, Stephen A. Morin, Adam A. Stokes, Aaron D. Mazzeo, Xin Chen, Michael Wang, George M. Whitesides. Multigait soft robot. *Proceedings of the National Academy of Sciences of the United States of America*, 108 (51), 20400-20403, 2011.

17. Janna C. Nawroth, Hyungsuk Lee, Adam W Feinberg, Crystal M. Ripplinger, Megan L. McCain, Anna Grosberg, John O. Dabiri, Kevin Kit Parker. *Nature Biotechnology*, 30(8), 792-799, 2012.

18. Shanshan Yao, Yong Zhu. Nanomaterial-Enabled Stretchable Interconnects: Strategies, Materials and Devices. *Advanced Materials*, 27, 1480-1511, 2015.

19. Tahmina Akter, Woo Soo Kim. Reversibly Stretchable Transparent Conductive Coatings of Spray-Deposited Silver Nanowires. *ACS Applied Materials and Interfaces*, 4, 1855-1859, 2012.

20. Le Cai, Jinzhu Li, Pingshan Luan, Haibo Dong, Duan Zhao, Qiang Zhang, Xiao Zhang, Min Tu, Qingsheng Zeng, Weiya Zhou, Sishen Xie. Highly Transparent and

Conductive Stretchable Interconnects Based on Heirarchical Reticulate Single-Walled Carbon Nanotube Architecture. *Advanced Functional Nanomaterials*, 22, 5238-5244, 2012.

21. Cunjiang Yu, Charan Masarapu, Jiepeng Rong, Bingqing Wei, Hanqing Jiang. Stretchable Supercapacitors Based on Buckled Single-Walled Carbon Nanotube Macrofilms. *Advanced Materials*, 21, 4793-4797, 2009.

22. Takehiro Tokuno, Masaya Nogi, Jinting Jiu, Katsuaki Suganuma. Hybrid transparent electrodes of silver nanowires and carbon nanotubes: a low-temperature solution process. *Nanoscale Research*, 7, 281-288, 2012.

23. Jinhwan Lee, Phillip Lee, Hyungman Lee, Dongjin Lee, Seung Seob Lee, Seung Hwan Ko. Very ling Ag nanowire synthesis and its application in a highly transparent, conductive and flexible metal electrode touch panel. *Nanoscale*, 4, 6408-6414, 2012.

24. Erik C. Garnett, Wenshan Cai, Judy J. Cha, Fakhruddin Mahmood, Stephen T. Connor, M. Greyson Christoforo, Yi Cui, Michael D. McGeheeMark L. Brongersma. Self-limited plasmonic welding of silver nanowire junctions. *Nature Materials*, 11, 241-249, 2012.

25. Jiajie Liang, Lu Li, Kwing Tong, Zhi Ren, Wei Hu, Xiaofan Niu, Yongsheng Chen, Qibing Pei. *ACS Nano*, 8(2), 1590-1600, 2014.

26. Seungyong Han, Sukjoon Hong, Jooyeun Ham, Junyeob Yeo, Jinhwan Lee, Bongchul Kang, Phillip Lee, Jinhyeong Kwon, Seung S. Lee, Min-Yang Yang, Seung Hwan Ko. Fast Plasmonic Laser Nanowelding for a Cu-Nanowire Percolation Network for Flexible Transparent Interconnects and Stretchable Electronics. *Advanced Materials*, 26, 5808-5814, 2014.

27. Ju Yeon Woo, Kyun Kyu Kim, Jongsoo Lee, Ju Tae Kim, Chang-Soo Han. Highly conductive and stretchable Ag nanowire/carbon nanotube hybrid interconnects. *Nanotechnology*, 25, 285203-285210, 2014.

28. Shanshan Yao, Yong Zhu. Wearable multifunctional sensors using printed stretchable interconnects made of silver nanowires. *Nanoscale*, 6, 2345-2352, 2014.
29. Akash Shankar, Eduardo Salcedo, Aaron Berndt, Daniel Choi, Jong Eun Ryu. Pulsed light sintering of silver nanoparticles for large deformation of printed stretchable electronics. *Advanced Composites and Hybrid Materials*, 1, 193-198, 2018.

30. Inhyuk Kim, Kyoohee Woo, Zhaoyang Zhong, Pyungsam Ko, Yunseok Jang, Minhun Jung, Jeongdai Jo, Sin Kwon, Seung-Hyun Lee, Sungwon Lee, Hongseok Youn, Jooho Moon. A photonic sintering derived Ag flake/nanoparticle-based

highly sensitive stretchable strain sensor for human motion monitoring. *Nanoscale*, 10, 7890-7897, 2018.

31. Changyong Yim, Zachary A. Kockerbeck, Sae Byeok Jo, Simon S. Park. Hybrid Copper-Silver-Graphene Nanoplatelet Conductive Inks on PDMS for Oxidation Resistance Under Intensive Pulsed Light. *ACS Applied Materials & Interfaces*, 9, 37160-37165, 2017.

32. Hyun-Jun Jeong, Hyun-Mo Lee, Chung-Hyeon Ryu, Eun-Jae Park, Ki-Lim Han, Hyun-Jun Hwang, Kyung-Chul Ok, Hak-Sung Kim, Jin-Seong Park. Ultra-High-Speed Intense Pulsed-Light Irradiation Technique for High-Performance Zinc Oxynitride Thin-Film Transistors. *ACS Applied Materials & Interfaces*, 11(4), 4152-4158, 2019.

33. Audrey Moores, Fre'de´ric Goettmann. The plasmon band in noble metal nanoparticles: an introduction to theory and applications. *RSC New Journal of Chemistry*, 30, 1121-1132, 2006.

34. K. Lance Kelly, Eduardo Coronado, Lin Lin Zhao, George C. Schatz. The Optical Properties of Metal Nanoparticles: The Influence of Size, Shape, and Dielectric Environment. *RSC Journal of Physical Chemistry B*, 107(3), 668-677, 2003.

35. Jin Z. Zhang, Cecilia Noguez. Plasmonic Optical Properties and Applications of Metal Nanostructures. *Plasmonics*, 3(4), 127-150, 2008.

36. Sebastian Wünscher, Robert Abbel, Jolke Perelaer, Ulrich S. Schubert. *RSC Journal of Materials Chemistry C*, 2, 10232-10261, 2014.

37. Yeon-Taek Hwang, Wan-Ho Chung, Yong-Rae Jang, Hak-Sung Kim. Intensive Plasmonic Flash Light Sintering of Copper Nanoinks Using a Band-Pass Light Filter for Highly Electrically Conductive Electrodes in Printed Electronics. *ACS Applied Materials & Interfaces*, 8(13), 8591-8599, 2016.

38. Gyung-Hwan Oh, Hyun-Jun Hwang, Hak-Sung Kim. Effect of copper oxide shell thickness on flash light sintering of copper nanoparticle ink. *RSC Advances*, 7(29), 17724-17731, 2017.

39. Sung-Jun Joo, Sung-Hyeon Park, Chang-Jin Moon, Hak-Sung Kim. A Highly Reliable Copper Nanowire/Nanoparticle Ink Pattern with High Conductivity on Flexible Substrate Prepared via Flash Light-Sintering Technique. *ACS Applied Materials & Interfaces*, 7(10), 5674-5684, 2015.

40. Myeong-Hyeon Yu, Sung-Joon Ju, Hak-Sung Kim. Multi-pulse flash light sintering of bimodal Cu nanoparticle-ink for highly conductive printed Cu electrodes. *Nanotechnology*, 28, 205205-205216, 2017.

41. Shalu Bansal, Chih-Hung Chang, Rajiv Malhotra. The Coupling Between Densification and Optical Heating in Intense Pulsed Light Sintering of Silver Nanoparticles. *ASME 2016 11th International Manufacturing Science and Engineering Conference*, 1, 8693-8700, 2016.

42. Yulia Galagan, Erica W. C. Coenen, Robert Abbel, Tim J. van Lammeren, Sami Sabik, Marco Barink, Erwin R. Meinders, Ronn Andriessen, Paul W.M. Blom. Photonic sintering of inkjet printed current collecting grids for organic solar cell applications. *Organic Electronics*, 14(1), 38-46, 2013.

43. T. Björninen, J. Virkki, L. Sydänheimo, L. Ukkonen. Manufacturing of Antennas for Passive UHF RFID Tags by Direct Writ Dispensing of Copper and Silver Inks on Textiles. *IEEE Explore*, 978-1-4799-7806-9/15, 589-592, 2015.

44. Shalu Bansal, Rajiv Malhotra. Nanoscale-shape-mediated coupling between temperature and densification in intense pulsed light sintering. *Nanotechnology*, 27, 495602-495618, 2016.

45. Michael Dexter, Andrew Pfau, Zhongwei Gao, Gregory S. Herman, Chih-hung Chang, Rajiv Malhotra. Modelling nanoscale temperature gradients and conductivity evolution in pulsed light sintering of silver nanowire networks. *Nanotechnology*, 29, 505205-505220, 2018.

46. Ho Sun Lim, Soo Jin Kim, Ho Won Jang, Jung Ah Lim. Intense pulsed light for split-second structural development of nanomaterials. *RSC Journal of Material Chemistry C*, 5, 7142-7160, 2017.

47. Michael Zenou, Oleg Ermak, Amir Saar, Zvi Kotler. Laser sintering of Copper Nanoparticles. *Journal of Physics D : Applied Physics*, 47 (2), 025501-025512, 2014.

48. Hyun-Jun Hwang, Kyung-Hwan Oh, Hak-Sung Kim. All-photonic drying and sintering process via flash white-light combined with deep-UV and near-infrared irradiation for highly conductive copper nano-ink. *Nature: Scientific Reports*, 6, 19696-19706, 2016.

49. Ethan B. Secor. Guided ink and process design for aerosol jet printing based on annular drying effects. *IOP: Flexible and Printed Electronics*, 3, 35007-35016, 2018.

50. Fan Cai, Spyridon Pavlidis, John Papapolymerou, Yung Hang Chang, Kan Wang, Chuck Zhang, Ben Wang. Aerosol Jet Printing for 3-D Multilayer Passive Microwave Circuitry. *IEEE Explore: Proceedings of the 44th European Microwave Conference*, 512-516, 2014.
51. Michael D. Dickey. Emerging applications of Liquid Metals Featuring Surface Oxides. *ACS Applied Materials and Interfaces*, 6 (21), 18369-18379, 2014.

52. Dong Jun Lee, Sung Hyeon Park, Shin Jang, Hak Sung Kim, Je Hoon Oh, Yong Won Song. Pulsed light sintering characteristics of inkjet-printed nanosilver films on a polymer substrate. *Journal of Micromechanics and Microengineering*, 21, 125023-125030, 2011.
53. Hyun-Jun Hwang, Rajiv Malhotra. Shape-Tuned Junction Resistivity and Self-Damping Dynamics in Intense Pulsed Light Sintering of Silver Nanostructure Films. *ACS Advanced Materials and Interfaces*, 11, 3536-3546, 2019.